

Calibration methods and results for ExoMars/NOMAD SO and LNO

Giuliano Liuzzi and Geronimo L. Villanueva

NASA Goddard Space Flight Center, 20771 Greenbelt, MD, USA

Last modified date: August 28th, 2017

Table of Contents

1. Introduction	- 3 -
1.1. Instrument general configuration	- 3 -
1.2. Observation modes: SO and LNO channels	- 3 -
1.3. Diffraction orders overlapping	- 4 -
2. Observations and datasets	- 5 -
2.1. List of calibrations	- 5 -
2.2. NOMAD observations list and types	- 6 -
3. Calibrations	- 8 -
3.1. Wavenumber vs. pixel and order – Grating equation solution	- 8 -
3.1.1. <i>Principles and aims</i>	- 8 -
3.1.2. <i>Filtering mechanisms</i>	- 9 -
3.1.3. <i>Results</i>	- 10 -
3.2. Temperature dependency of wavenumber calibrations	- 14 -
3.2.1. <i>Temperature effects correction</i>	- 14 -
3.2.2. <i>Results</i>	- 15 -
3.3. Wavenumber vs. AOTF frequency calibration and AOTF transfer function	- 16 -
3.3.1. <i>Principles and implementation</i>	- 16 -
3.3.2. <i>Results: Wavenumber vs. AOTF frequency relation</i>	- 18 -
3.3.3. <i>Results - AOTF transfer function shape</i>	- 20 -
4. Spectral continuum modeling	- 21 -
4.1. Blaze function	- 21 -
4.2. Structure of the spectral continuum	- 22 -
4.3. Synthetic spectra sample calculations	- 26 -
5. Conclusions and future work	- 29 -
References	- 30 -
Appendix A – Calibration coefficients	- 30 -
Appendix B – AOTF optimal frequencies table	- 30 -

1. Introduction

The following document summarizes all the procedures developed and accomplished to perform the calibration of NOMAD instrument in the infrared channels, and the related scientific bases. All these procedures are based on the exploitation of data acquired during the Mars Capture Orbit-1 (MCO-1, November 2016), in order to evaluate the behavior of the instrument in flight, disregarding of previous ground-based calibrations.

In this introduction section, it is briefly described the instrument structure and observation geometries, and the mechanism used to select the diffraction order to observe, besides a synthetic characterization of how observed diffraction orders overlap. Also, a list of the calibration procedures developed for the instrument is presented.

1.1. Instrument general configuration

The Nadir and Occultation for MArS Discovery instrument (NOMAD) design is essentially based on that of the SOIR spectrometer [1,2] on board of Venus Express. The concept is that of a compact echelle grating spectrometer, which is combined with an Acousto-Optical Tunable Filter (AOTF) devoted to the pre-selection of the diffraction order to be observed. This is done by coupling the AOTF filter with a radio frequency generator, which modifies the diffraction properties of the AOTF as the input radio frequency varies. Since the AOTF is a narrow bandpass filter, this yields to vary the central frequency at which the AOTF transfer function peaks, and consequently the selection of the diffraction order that falls within the detector. The procedure to calibrate the response function of the AOTF filter and the wavenumber calibration will be explained in Section 3.

1.2. Observation modes: SO and LNO channels

The IR channels of NOMAD operate in two different configurations: The Solar Occultation (SO) and Limb and Nadir Observation (LNO). The first one works in the same way as that previously operated by SOIR [3], observing the solar radiation as it is attenuated by Martian atmosphere at different altitudes. The slit of the SO channel selects only a thin slice of the solar disk, and the optical scheme is the exact replica of that adopted in SOIR, and Figure 1 and Figure 2 summarize the SO observing geometry. Since NOMAD is operated on board of ExoMars on a polar orbit, the instrument can ideally perform two SO observations per orbit (ingress and egress occultations). The theoretical spectral interval of operation in SO configuration is $2.3 - 4.3 \mu\text{m}$ ($2325 - 4348 \text{ cm}^{-1}$), with a theoretical resolving power of ~ 20000 .

The LNO operation mode is instead conceived to observe the planet in a nadir or limb geometry, looking at the surface of the planet at different angles (Figure 1). This implies that the signal to be detected is much weaker than that observed in SO occultations, yielding the need of introducing some modifications in the instrumental setting. In particular, the LNO channel is characterized by a larger entrance slit, as well as most of the optical elements. Apart from the geometrical details, a much longer integration time (15 s against 4 ms in SO mode) is needed to raise at ~ 1000 the signal to noise ratio in LNO geometry. Further details are in [3]. The reduction of the signal and the challenging enhancement of the SNR value for LNO has some counterparts in the theoretical spectral interval of operation of the instrument, reduced to $2.3 - 3.8 \mu\text{m}$ ($2630 - 4348 \text{ cm}^{-1}$), with a theoretical resolving power of ~ 15000 . For the purposes of the calibration operations described in this document, it has to be stressed that these differences, together with the fact that SO and LNO use a different AOTF filter, force to treat separately SO and LNO observations. In particular, LNO observations are totally new with respect to the heritage of SOIR, on which the SO configuration is based.

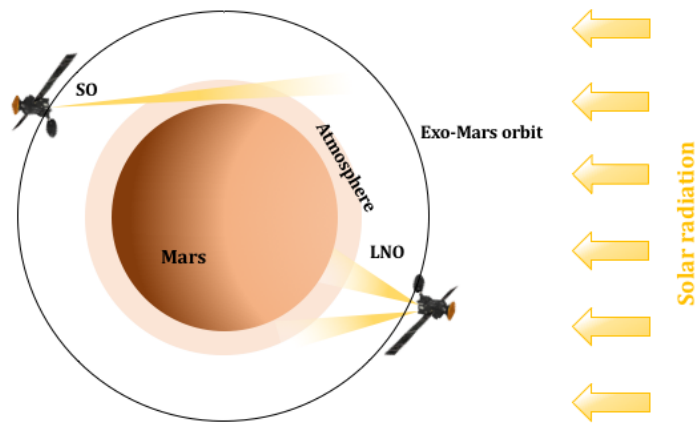


Figure 1 - Overview of the NOMAD SO and LNO viewing geometry. For the LNO, the scheme reports both the pictures of nadir and limb geometry.

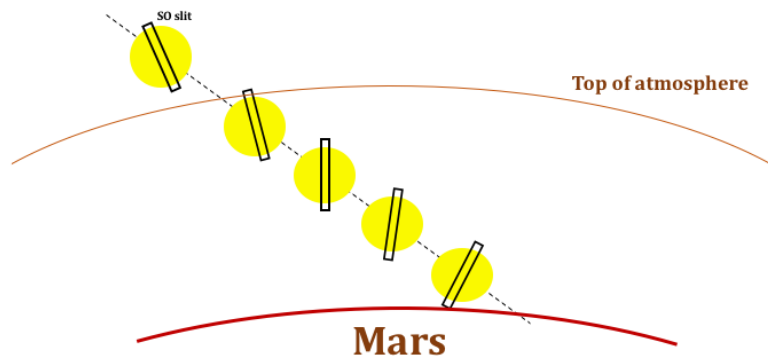


Figure 2 - Scheme of a typical SO observation: the slit rotates with respect to the perpendicular to the surface as the altitude of Sun and Line of Sight (LOS) changes. The slit is typically larger than the Sun disk.

1.3. Diffraction orders overlapping

The way in which the instrument selects the diffraction orders, through the AOTF, causes the different orders to overlap in the observed NOMAD spectrum. Indeed, despite the AOTF transfer function has been optimized in such a way to fit the filter bandpass to the Free Spectral Range (FSR) of the instrument, a consistent part of the observed flux has been found to come from the nearby orders. The quantification of these effects is left to a more thorough treatment in Section 3, where the AOTF function derivation procedure is described in every detail. Here it has to be pointed out that it has been found that, both SO and LNO calibration measurements indicate that, in order to correctly reproduce the observed spectrum, it is needed to take into account the flux coming from ± 3 orders around the central order selected by AOTF; moreover, the nearby orders contribution to the total flux is up to 40% of the total flux observed by the instrument. The amount of flux coming from the central and nearby orders is critically dependent on the position of the center of the AOTF bandpass with respect to the central frequency of the observed diffraction order: this concept is exemplified in Figure 3, where it is shown how, in case the AOTF function is not centered with respect to the order, the flux coming from other orders becomes very

significant, and degrades the quality of measurements. In this scheme, we assume for simplicity that AOTF function can be represented by a sinc squared function.

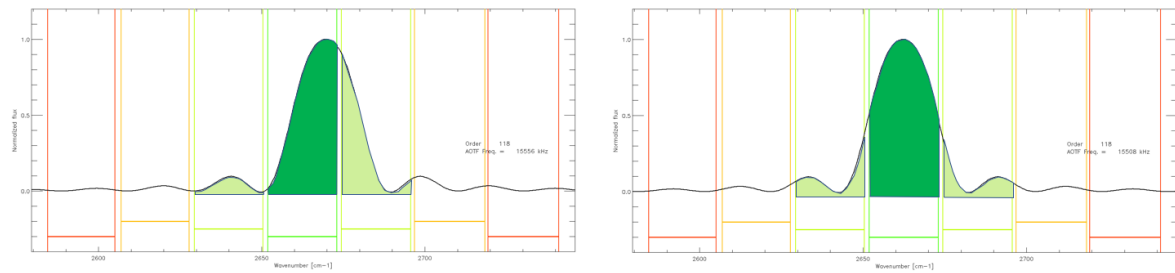


Figure 3 - Example of variation of order overlapping and variation of contribution from side orders. In the first case (left panel) the AOTF transfer function is shifted with respect to the order center, yielding an invasive contamination by the shortwave nearby order. The flux from nearby orders is minimized if the AOTF input radio frequency is chosen in order to center the AOTF transfer function with respect to the observed order (right panel). The data are extracted from actual NOMAD MCO-1 dataset (acquisition date: 23rd November, 2016).

2. Observations and datasets

The observations set for the calibration procedures presented here has been acquired during the MCO-1 phase. All the observations considered are calibration measurements, in which the instrument points directly to the Sun, both in SO and LNO configurations, while no observation has been performed to measure the atmospheric transmittance. A minor part of the available dataset, instead, consists of nadir observations, both night- and day-time, which have not been used in the present work.

As already said, the spectral interval measured in the two configurations is slightly different: in the case of SO, the instrument spans the interval 1.96 – 4.62 μm (2160-5095 cm^{-1}), which corresponds to the diffraction orders from 96 to 225, varying the AOTF input radio frequency from ~ 12300 to ~ 31100 kHz. In the LNO configuration, instead, this interval reduces to 2.00 – 4.12 μm (2430 – 4985 cm^{-1}), corresponding to the diffraction orders 108-220, scanned varying the AOTF frequency from ~ 14150 to ~ 32100 kHz. In both cases, the spectral interval exceeds that already experienced with SOIR, hence the results deriving from spectral and AOTF transfer function calibrations are expected to differ significantly from those already reckoned for SOIR.

2.1. List of calibrations

In this document results are reported for the following calibration procedures, specifically tailored on the data acquired in-flight by NOMAD:

- 1) Wavenumber vs. pixel calibration – grating equation solution
- 2) Wavenumber vs. AOTF frequency calibration
- 3) AOTF transfer function shape derivation
- 4) Spectral continuum definition vs. AOTF frequency
- 5) Nearby orders contamination estimation
- 6) Thermal effects on wavenumber calibration at 1)

2.2. NOMAD observations list and types

According to the system configuration (SO or LNO), to the target, and to the way in which input AOTF frequency is tuned, the following types of NOMAD observations have been performed during the MCO-1 phase:

- **Full Scan (F):** The Trace Gas Orbiter (TGO) points the NOMAD nadir boresights to nadir (in LNO) or the Sun through the atmosphere (SO) during this observation, and the AOTF input frequency is varied by large steps (~160 kHz) to perform a sweep over its complete spectral range, one diffraction order at a time. These measurements have not been employed for calibration purposes in this work, but have been used as test datasets for the solutions obtained. Although, in principle, the target of these observations is the planet, those available in the MCO-1 phase are calibration measurements, in which the instruments points directly the Sun.
- **Miniscan (M):** The NOMAD SO and LNO channels perform a sweep over a fraction of their spectral range whilst pointing towards the sun. To do this, the AOTF input frequency is slowly varied (at steps of a few kHz), in order to observe the behavior of the observed signal across different orders and in the transition between them. These are the observations that have been actually employed for the calibration procedures described in this document.
- **Day nadir (D):** The NOMAD LNO channels observe pointing the TGO towards the center of Mars, perpendicular to the surface directly underneath it. Sun is positioned such that the surface is illuminated. These are standard science measurements where a small selection of diffraction orders is cycled through repeatedly. This is the baseline science observation during a nadir. The available (D) type observations have been used as test data to probe the accuracy of the wavenumber calibration and the algorithm to build the shape of the continuum.
- **Night nadir (N):** Same as (D), but in this case the surface target is positioned on the night side of the planet. Due to the very low signal to noise ratio, this kind of observations has been considered neither in the calibration procedures, nor in the validation of results.
- **Other calibration measurements (C),** in which the instrument points directly the Sun, performing a series of observations in which the AOTF frequency is kept fixed (single order observations).

The list of observations used for calibration aims, both for SO and LNO, is reported in Table 1.

#	FILENAME	TYPE	INST	INST. T (°C)	AOTF FREQ. (kHz)	ORDERS
S1	20161121_012420_SO_C.h5	C	SO	-9.961, -8.058	21684	160
S2	20161121_030950_SO_C.h5	C	SO	-6.766, -5.768	15842	120
S3	20161121_033050_SO_C.h5	C	SO	-5.315, -4.755	15842	120
S4	20161121_193450_SO_C.h5	C	SO	-8.388, -7.355	20373	151
S5	20161121_224950_SO_C.h5	F	SO	-19.080, -14.507	12386 - 31086	96 - 225
S6	20161122_010950_SO_C.h5	M	SO	-13.430, -12.460	12757 - 13267	99 - 102
S7	20161122_012950_SO_C.h5	M	SO	-12.180, -11.347	13199 - 13709	102 - 105
S8	20161122_014950_SO_C.h5	M	SO	-11.283, -10.593	14962 - 15472	114 - 117
S9	20161122_030950_SO_C.h5	M	SO	-10.816, -9.868	16281 - 16791	123 - 126
S10	20161122_035050_SO_C.h5	M	SO	-9.495, -8.504	13640 - 14150	105 - 108
S11	20161122_223450_SO_C.h5	M	SO	-15.735, -14.859	20665 - 21175	153 - 156
S12	20161122_231550_SO_C.h5	M	SO	-14.298, -13.178	22411 - 22921	165 - 168
S13	20161123_003550_SO_C.h5	M	SO	-13.286, -12.216	24154 - 24664	177 - 180
S14	20161123_011550_SO_C.h5	M	SO	-12.159, -10.708	26327 - 26837	192 - 195

S15	20161123_023550_SO_C.h5	M	SO	-11.003, -9.976	15402 - 15912	117 - 120
S16	20161123_031550_SO_C.h5	M	SO	-9.602, -8.554	18476 - 18986	138 - 141
S17	20161123_150450_SO_C.h5	M	SO	-10.098, -9.250	21539 - 22049	159 - 162
S18	20161123_154550_SO_C.h5	M	SO	-9.100, -8.087	22847 - 23357	168 - 171
S19	20161123_170550_SO_C.h5	M	SO	-8.798, -7.793	24589 - 25099	180 - 183
S20	20161123_174550_SO_C.h5	M	SO	-7.506, -6.773	14081 - 14591	108 - 111
S21	20161123_190550_SO_C.h5	M	SO	-7.434, -6.407	15842 - 16352	120 - 123
S22	20161123_194550_SO_C.h5	M	SO	-6.235, -5.265	20228 - 20738	150 - 153
S23	20161123_223450_SO_C.h5	M	SO	-13.817, -12.834	21975 - 22485	162 - 165
S24	20161123_231550_SO_C.h5	M	SO	-12.489, -11.369	23283 - 23793	171 - 174
S25	20161125_153450_SO_C.h5	M	SO	-9.229, -8.418	23719 - 24229	174 - 177
S26	20161125_161550_SO_C.h5	M	SO	-9.875, -7.369	28494 - 29004	207 - 211
S27	20161125_173550_SO_C.h5	M	SO	-7.994, -7.096	14521 - 15031	111 - 114
S28	20161125_181550_SO_C.h5	M	SO	-6.874, -6.005	17160 - 17670	129 - 132
S29	20161125_193550_SO_C.h5	M	SO	-6.838, -5.983	17599 - 18109	132 - 135
S30	20161125_201550_SO_C.h5	M	SO	-5.825, -4.906	18038 - 18548	135 - 138
S31	20161127_150450_SO_C.h5	M	SO	-9.121, -8.748	19352 - 19862	144 - 147
S32	20161127_154550_SO_C.h5	M	SO	-8.216, -7.182	19790 - 20300	147 - 150
S33	20161127_170550_SO_C.h5	M	SO	-10.902, -7.326	25024 - 25534	183 - 186
S34	20161127_190550_SO_C.h5	M	SO	-10.234, -6.220	26761 - 27271	195 - 198
S35	20161127_194550_SO_C.h5	M	SO	-9.480, -5.122	27195 - 27705	198 - 201
S36	20161127_211950_SO_C.h5	C	SO	-8.238, -7.154	21684	160

L1	20161121_000420_LNO_C.h5	C	LNO	-39.760, -12.539	22946	160
L2	20161121_021920_LNO_C.h5	C	LNO	-18.563, -11.203	22946	160
L3	20161121_183450_LNO_C.h5	C	LNO	-12.654, -12.323	16749	120
L4	20161121_185450_LNO_C.h5	C	LNO	-12.582, -12.316	16749	120
L5	20161121_191450_LNO_C.h5	C	LNO	-12.316, -12.007	16749	120
L6	20161121_233000_LNO_C.h5	F	LNO	-22.822, -17.558	14150 - 32130	108 - 220
L7	20161122_020950_LNO_C.h5	M	LNO	-15.117, -14.736	15814 - 16324	114 - 117
L8	20161122_033050_LNO_C.h5	M	LNO	-13.925, -13.630	17215 - 17725	123 - 126
L9	20161122_153906_LNO_D_169.h5	D	LNO	-11.700, -9.400	24332	169
L10	20161122_225550_LNO_C.h5	M	LNO	-34.131, -19.166	21866 - 22376	153 - 156
L11	20161122_235550_LNO_C.h5	M	LNO	-27.704, -17.867	23716 - 24226	165 - 168
L12	20161123_005550_LNO_C.h5	M	LNO	-19.310, -16.423	25562 - 26072	177 - 180
L13	20161123_013550_LNO_C.h5	M	LNO	-15.404, -14.743	27861 - 28371	192 - 195
L14	20161123_025550_LNO_C.h5	M	LNO	-14.118, -13.817	16281 - 16791	117 - 120
L15	20161123_033550_LNO_C.h5	M	LNO	-12.984, -12.582	19545 - 20055	138 - 141
L16	20161123_152550_LNO_C.h5	M	LNO	-32.766, -12.481	22792 - 23302	159 - 162
L17	20161123_160550_LNO_C.h5	M	LNO	-18.700, -11.943	24178 - 24688	168 - 171
L18	20161123_172550_LNO_C.h5	M	LNO	-12.359, -11.677	26022 - 26532	180 - 183
L19	20161123_180550_LNO_C.h5	M	LNO	-10.916, -10.593	14878 - 15388	108 - 111
L20	20161123_192550_LNO_C.h5	M	LNO	-10.557, -10.284	16749 - 17259	120 - 123
L21	20161123_200550_LNO_C.h5	M	LNO	-17.443, -9.329	21402 - 21912	150 - 153
L22	20161123_225550_LNO_C.h5	M	LNO	-30.397, -17.903	23254 - 23764	162 - 165
L23	20161123_233550_LNO_C.h5	M	LNO	-20.574, -15.799	24640 - 25150	171 - 174
L24	20161125_155550_LNO_C.h5	M	LNO	-15.411, -11.943	25101 - 25611	174 - 177
L25	20161125_163550_LNO_C.h5	M	LNO	-11.296, -11.031	30151 - 30661	207 - 210
L26	20161125_175550_LNO_C.h5	M	LNO	-11.196, -10.923	15346 - 15856	111 - 114
L27	20161125_183550_LNO_C.h5	M	LNO	-10.291, -10.011	18148 - 18658	129 - 132
L28	20161125_195550_LNO_C.h5	M	LNO	-10.033, -9.832	18614 - 19124	132 - 135
L29	20161125_203550_LNO_C.h5	M	LNO	-9.264, -8.927	19080 - 19590	135 - 138
L30	20161126_220850_LNO_D_190.h5	D	LNO	-10.378, -8.403	27555	190
L31	20161127_152550_LNO_C.h5	M	LNO	-12.675, -11.282	20474 - 20984	144 - 147
L32	20161127_160550_LNO_C.h5	M	LNO	-14.140, -11.160	20938 - 21448	147 - 150
L33	20161127_172550_LNO_C.h5	M	LNO	-13.106, -11.189	26482 - 26992	183 - 186
L34	20161127_180550_LNO_C.h5	M	LNO	-11.720, -10.054	26942 - 27452	186 - 189
L35	20161127_192550_LNO_C.h5	M	LNO	-9.925, -9.731	28319 - 28829	195 - 198
L36	20161127_200550_LNO_C.h5	M	LNO	-9.056, -8.776	28778 - 29288	198 - 201

Table 1 - List of the NOMAD MCO-1 observations used in the calibration procedure and/or validation and testing of the results. The first 8 characters in the filename indicate the date in which observations have been acquired.

It is important to stress that the observations of type D are eventually used only in the phase of testing the calibration results for LNO, while the observations of types C and F have been used both for testing the results and in the procedure to calibrate the dependency of wavenumber calibration on thermal effects. The other calibration procedures, instead, have been carried on with the sole usage of miniscans (M). Moreover, the temperatures reported in the table are the “SENSOR 1” temperatures (under ‘/Housekeeping/SENSOR_1_TEMPERATURE_SO-LNO’ field in the .h5 files), which have been recognized as more stable with respect to the other temperatures stored in data files.

An example of miniscan radiances is reported in the left panel of Figure 4. The most prominent solar features are well visible in the spectral pattern as absorption lines. Right panel, instead, shows an example of full scan. In this case, the transition between orders is not present because of the scanning mechanism (large AOTF frequency steps).

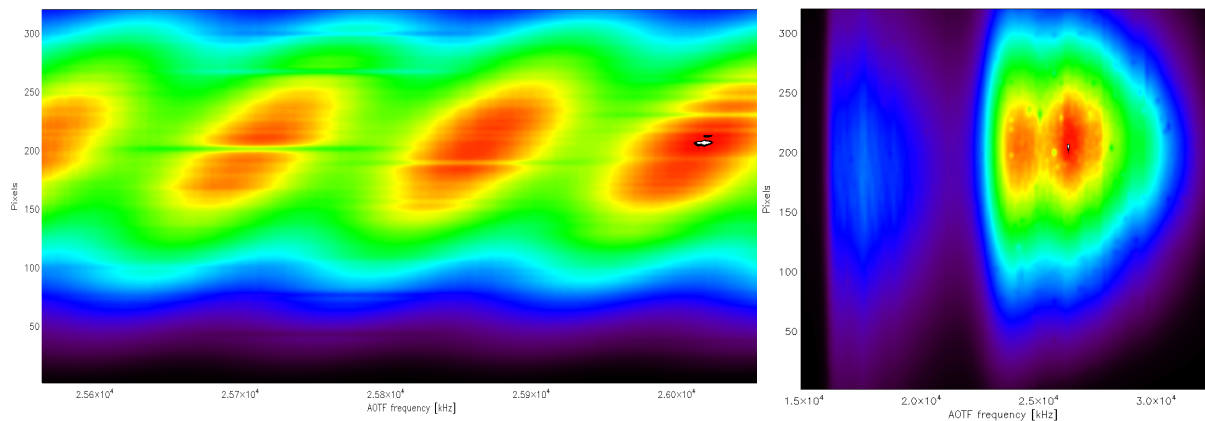


Figure 4 – Left panel: Example of miniscan data (file #L12 in Table 1). The intensity of the signal is represented by colors. Solar lines are evident as horizontal stripes. The transition between orders as AOTF frequency increases corresponds to the points, along X axis, in which the signal is low. Right panel: example of full scan data (file #L6 in Table 1). In this case, every column of the image represents a single spectrum, and a particular diffraction order. As before, the absorption due to solar lines is visible in the image, where it is also evident the variation of signal intensity with AOTF frequency across the entire spectral interval sounded by NOMAD (LNO in this case)

3. Calibrations

The calibration operations and procedures described here in the following have been conceived to be run sequentially and in synergy. The aim of these procedures is to obtain, for each date (or set of dates) in which calibration measurements are performed, a set of coefficients by which raw measurements can be calibrated in frequency and reproduced by radiative transfer models (i.e. the superposition between different diffraction orders is fully described). The structure of these coefficients will be illustrated at the end of this Section. All the procedures are implemented in IDL codes.

3.1. Wavenumber vs. pixel and order – Grating equation solution

3.1.1. Principles and aims

The aim of this calibration is to obtain an analytic relation between the pixel number of the detector, the diffraction order, and the corresponding wavenumber. In this process, the order number is not an independent variable, since it is fixed by AOTF input frequency A , which is the only independent variable in this calibration scheme, together with the pixel number. As a by-product of this process, an estimation of the resolving power of the instrument is also retrieved.

For the first run, the starting point for this (and the other calibrations) is assumed to be the parameterization retrieved from previous calibrations. The relation between pixel number p (from 0 to 319), wavenumber ν and order number m is modeled by a second-order polynomial of the form:

$$\frac{\nu}{m} = F_0 + F_1p + F_2p^2 \quad \text{Eq. 1}$$

while the polynomial relation between the AOTF frequency A and the wavenumber V at which AOTF bandpass is centered is

$$V = G_0 + G_1A + G_2A^2 \quad \text{Eq. 2}$$

The calibration principle works as follows. Exploiting the miniscan measurements (see Table 1), the procedure first compute the average of all the spectra whose AOTF frequency fall within the same diffraction order. This is done without the aid of another calibration relation (like order vs. AOTF frequency), but simply computing W from Eq. 2, and solving Eq. 1 with $V=\nu$ and $p=160$, the central pixel, and picking the *lower integer* of the result.

Then, within an iterative process, the observed spectrum \mathbf{S}_o is shifted in frequency (of an amount $\Delta\nu$) by regular steps (equal to the spectral sampling, i.e. one pixel), in order to seek for the best correlation between the whole spectrum \mathbf{S}_o and a synthetic solar spectrum \mathbf{S}_\odot computed on the same spectral interval, and between the part of the observed spectrum \mathbf{S}_{oL} that contains the brightest solar line and the synthetic one $\mathbf{S}_{\odot L}$. Hence, the two highest correlations, namely C_0 and C_L , are computed:

$$C_0 = \max(\text{corr}(\mathbf{S}_o, \mathbf{S}_\odot)) \quad \text{Eq. 3}$$

$$C_L = \max(\text{corr}(\mathbf{S}_{oL}, \mathbf{S}_{\odot L})) \quad \text{Eq. 4}$$

and the corresponding displacement $\Delta\nu$ with respect to the pre-computed calibration is the minimum of the two displacements corresponding to the two correlation values. The double correlation is finalized to make the procedure more robust to possible periodicity in the solar lines, or cases in which two solar features of similar intensities are comprised in few pixels. The output of this first step is a new spectral grid, denoted with $\mathbf{v}+\Delta\nu$.

Once this first step is performed, the actual wavenumber calibration is done locating on the spectrum the solar lines whose intensity exceeds a user-defined threshold; the pixel at which line is located is denoted as p_o . Each single line is then fitted by a simple Gaussian model, which defines the center of the line (in “absolute wavenumber” units, namely wavenumber divided by order, on the grid $\mathbf{v}+\Delta\nu$ – denoted with \mathbf{v}'), and its Full Width at Half Maximum (*FWHM*). An estimation for the three coefficients in Eq. 1 is then provided by fitting the relation between the center of the lines (values of p_o) and the wavenumbers of the same lines divided by the corresponding diffraction orders, \mathbf{v}_o/m , provided by the Gaussian fit, along with the corresponding errors. Moreover, for each of the line considered, the resolving power is:

$$RP = \frac{\nu_o}{FWHM} \quad \text{Eq. 5}$$

3.1.2. Filtering mechanisms

The first part of the procedure, in which NOMAD data are matched to solar synthetic spectra, the analysis excludes automatically the first 50 and last 10 pixels of NOMAD spectra, in which typically the signal is low.

Prior to fit the single lines with Gaussian profiles, the procedure creates a vector of errors, in which the position of the solar lines of the considered order and the two nearby orders, and the nearby ± 5 pixels are marked. In this way, the algorithm discards the line either if two or more solar lines above the selected threshold are too close to that (i.e. there are less than 7 “continuum”

pivot points in the 30 pixels around the line center), or if that line in the order is close to the ghost of another solar line in one of the nearby orders.

Furthermore, given the preliminary assessment of the spectral grid in the first phase, the analysis discards all the solar lines for which the retrieved center is not within 0.5 cm^{-1} the first guess.

3.1.3. Results

This calibration procedure is implemented in the fully automated (no human intervention needed during its operation) IDL procedure named *exofreq.pro*. The program takes the following input data: instrument (SO or LNO), the date (or multiple dates) of the observations to analyze, and the threshold for the solar lines intensity. The procedure outputs the set of coefficients F_0 , F_1 and F_2 of Eq. 1 for the miniscans in the selected date(s), and the average resolving power, computed on the basis of the analysis performed on the single solar lines. All the calculations shown here have been done using a solar line intensity threshold = 0.4.

Figure 5 to Figure 12 represent the results obtained using all the miniscans acquired in single dates. Each point in the plots correspond to the position (in pixels and “absolute” wavenumbers) of a single solar line, while its color indicates the diffraction order in which that solar line is observed. Bottom panel reports the residuals with respect to the retrieved tuning relation.

Figure 13 and Figure 14 represent the same kind of analysis obtained considering all the available miniscans from the dates 22nd, 23rd, 25th and 27th of November 2016. This more extensive analysis is needed to reckon a tuning relation on the whole spectral interval spanned by NOMAD, including lines coming from all the diffraction orders. The results presented in this collection of plots already embody the correction of spectral grids with instrumental temperatures, which is performed starting from the second run of the set of calibration procedures, and whose specifics and principles are described in Section 3.2.

The calibration coefficients found for each date are summarized in Table 2. In this case, since the observations span a restricted period of time, the fluctuations in the values are very limited. Nevertheless, the application of this calibration procedure to measurements acquired in different periods could be a way to monitor possible changes in the behavior of the instrument. The calibration coefficients for the tuning relation assumed for the following calibration steps and to perform radiative transfer calculations on NOMAD data are those retrieved using all the available miniscans (bold in Table 2

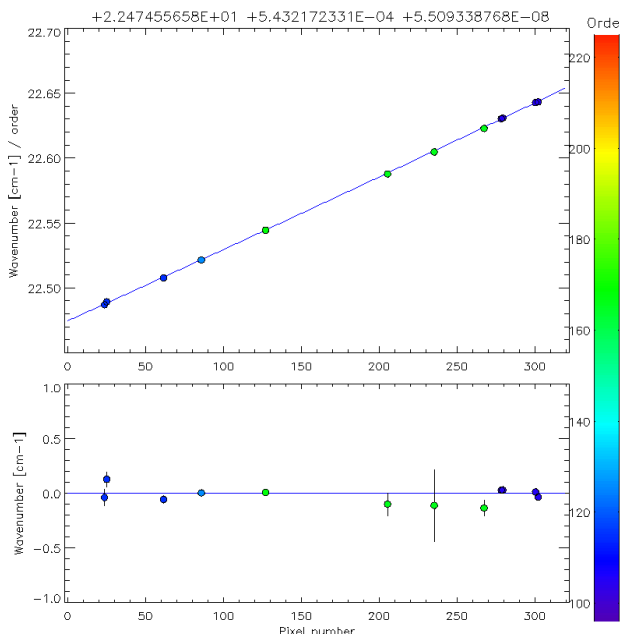


Figure 5 - Results for SO miniscans of 22nd November 2016 (files #S6 – S12).

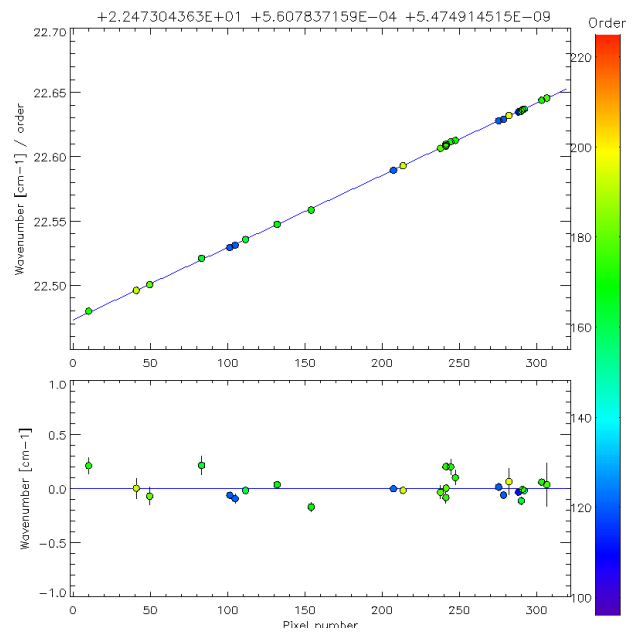


Figure 6 - Results for SO miniscans of 23rd November 2016 (files #S13 – S24).

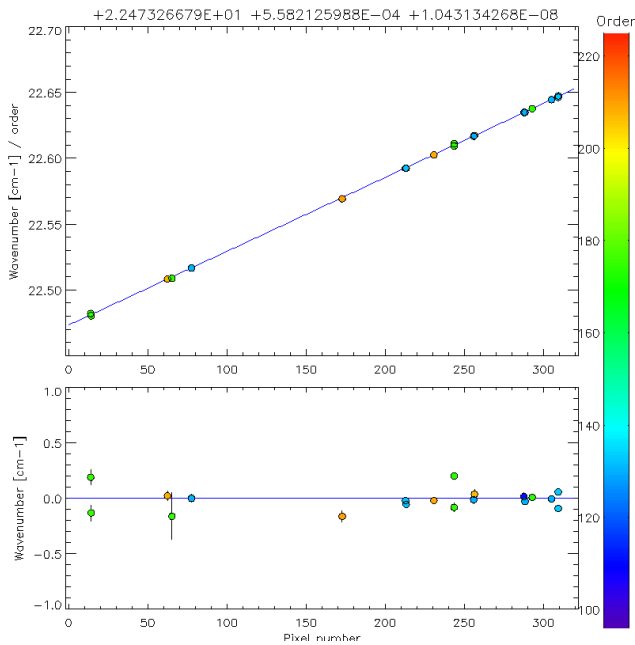


Figure 7 - Results for SO miniscans of 25th November 2016 (files #S25 – S30).

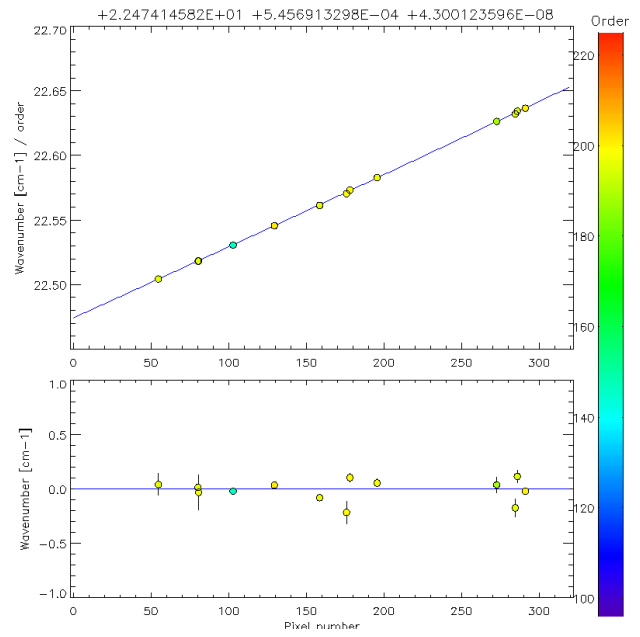


Figure 8 - Results for SO miniscans of 27th November 2016 (files #S31 – S36).

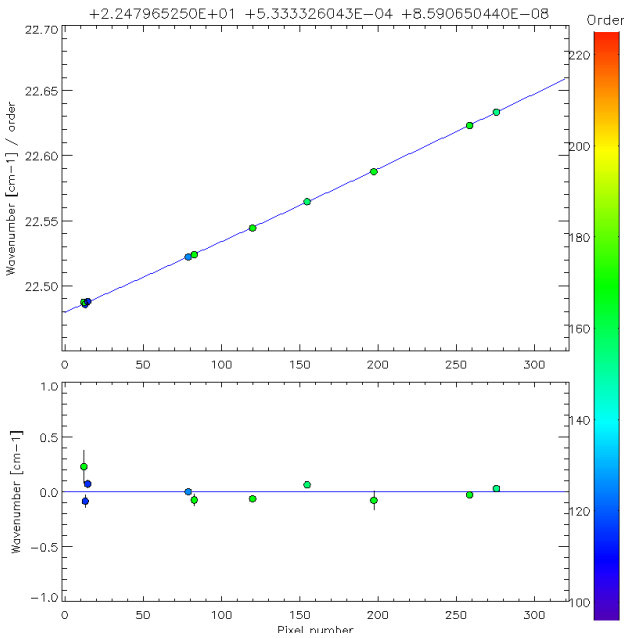


Figure 9 - Results for LNO miniscans of 22nd November 2016 (files #L7/8/10/11).

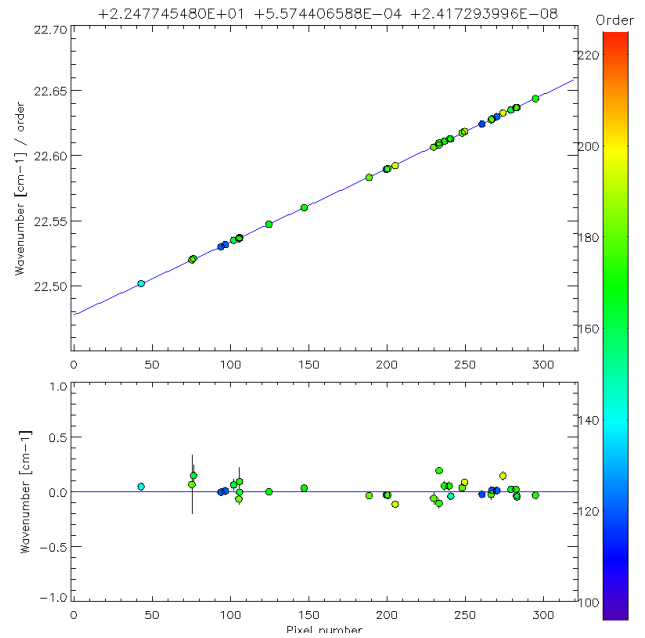


Figure 10 - Results for LNO miniscans of 23rd November 2016 (files #L12-L23).

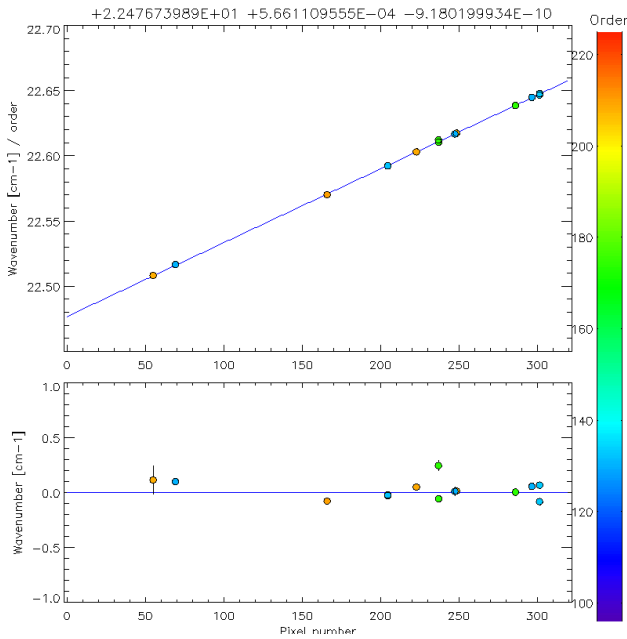


Figure 11 - Results for LNO miniscans of 25th November 2016 (files #L24-L29).

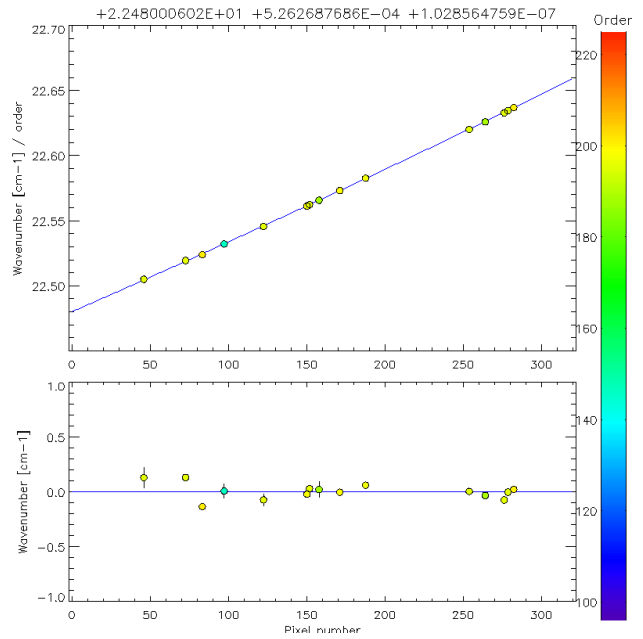


Figure 12 - Results for LNO miniscans of 27th November 2016 (files #L31-L36).

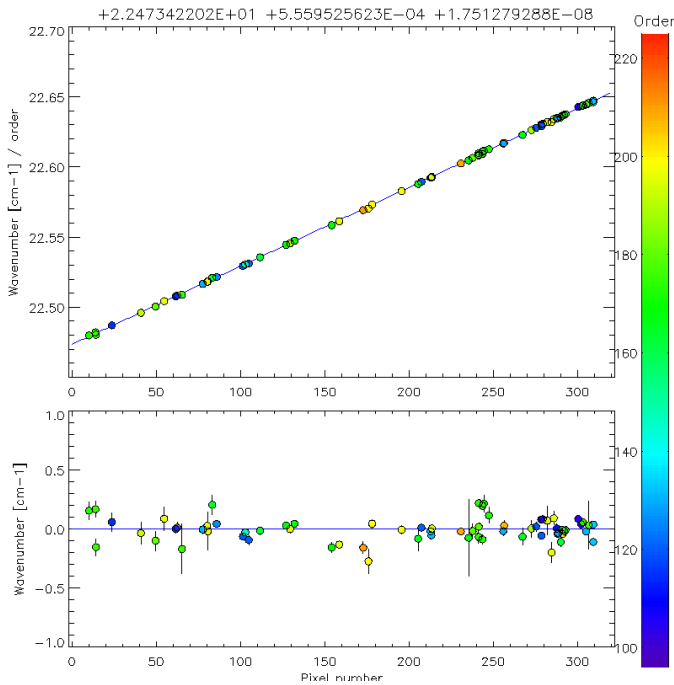


Figure 13 - Results for all SO miniscans of 22nd, 23rd, 25th and 27th November 2016.

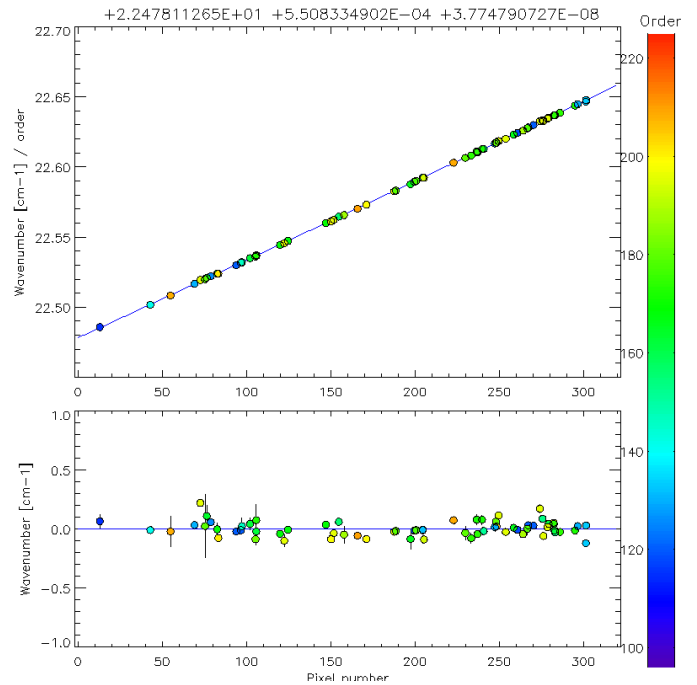


Figure 14 - Results for all LNO miniscans of 22nd, 23rd, 25th and 27th November 2016.

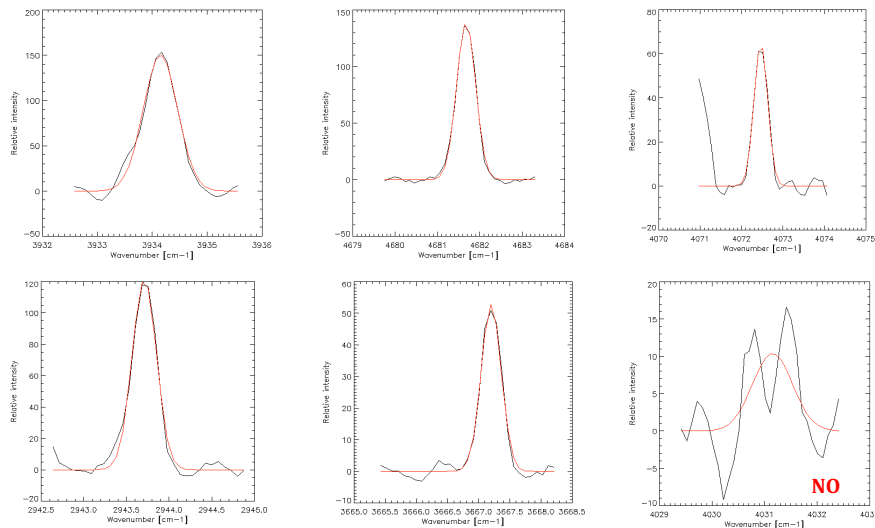
INSTRUMENT	DATE	F_0	F_1	F_2
SO	22 nd Nov. 2016	22.474557	$5.432172 \cdot 10^{-4}$	$5.509339 \cdot 10^{-8}$
SO	23 rd Nov. 2016	22.473044	$5.607837 \cdot 10^{-4}$	$5.474915 \cdot 10^{-9}$
SO	25 th Nov. 2016	22.473267	$5.582126 \cdot 10^{-4}$	$1.043134 \cdot 10^{-8}$
SO	27 th Nov. 2016	22.474146	$5.456913 \cdot 10^{-4}$	$4.300124 \cdot 10^{-8}$
LNO	22 nd Nov. 2016	22.479653	$5.333326 \cdot 10^{-4}$	$8.590650 \cdot 10^{-8}$
LNO	23 rd Nov. 2016	22.477455	$5.574407 \cdot 10^{-4}$	$2.417294 \cdot 10^{-8}$
LNO	25 th Nov. 2016	22.476740	$5.661110 \cdot 10^{-4}$	$-9.180200 \cdot 10^{-10}$
LNO	27 th Nov. 2016	22.480006	$5.262688 \cdot 10^{-4}$	$1.028565 \cdot 10^{-7}$
SO	All	22.473422	$5.559526 \cdot 10^{-4}$	$1.751279 \cdot 10^{-8}$
LNO	All	22.478113	$5.508335 \cdot 10^{-4}$	$3.774791 \cdot 10^{-8}$

Table 2 - Retrieved coefficients for the tuning relation. The last two rows report retrieved values using all the miniscan data available, reported in Table 1.

The second output of the procedure implemented in *exofreq.pro* is the resolving power of the instrument, retrieved from the parameters derived by Gaussian fits of the single solar lines. In this process, it is assumed that the line profile is independent of temperature, order, or pixel¹. The Gaussian fits, performed through the IDL procedure *gaussfit.pro*, is based on a non-linear least squares approach. Lines are divided by the local continuum, in order to fit the line profile with a simple Gaussian, without the addition of any continuum. Once the pre-filtering of lines is done, aimed to exclude possible double lines (Section 3.1.2), fits are considered valid only if:

- the fit converged
- the RP value for that line is $10^4 < RP < 3 \cdot 10^4$
- the line center is within 0.5 cm^{-1} the first guess
- the $FWHM > 3\chi^2\sigma$, with σ the error on the $FWHM$ retrieved value

Some examples of solar line fit are provided in Figure 15 and Figure 16. Results indicate that the SO configuration has a resolving power of ~ 19000 , while in LNO configuration the retrieved average resolving power is ~ 14000 .



¹ Some observations about this aspect will be provided in Conclusions section.

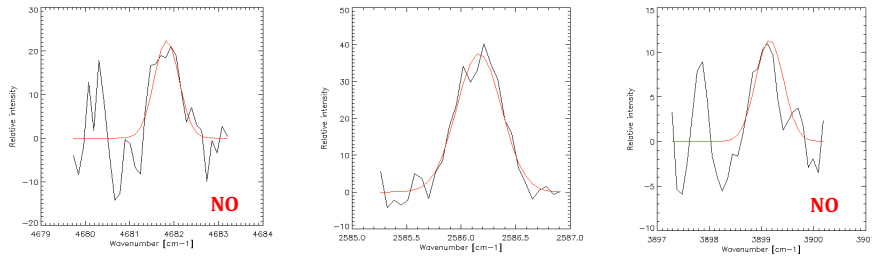


Figure 15 - Examples of solar lines from LNO observations. Those marked with a 'NO' are discarded from retrieval.

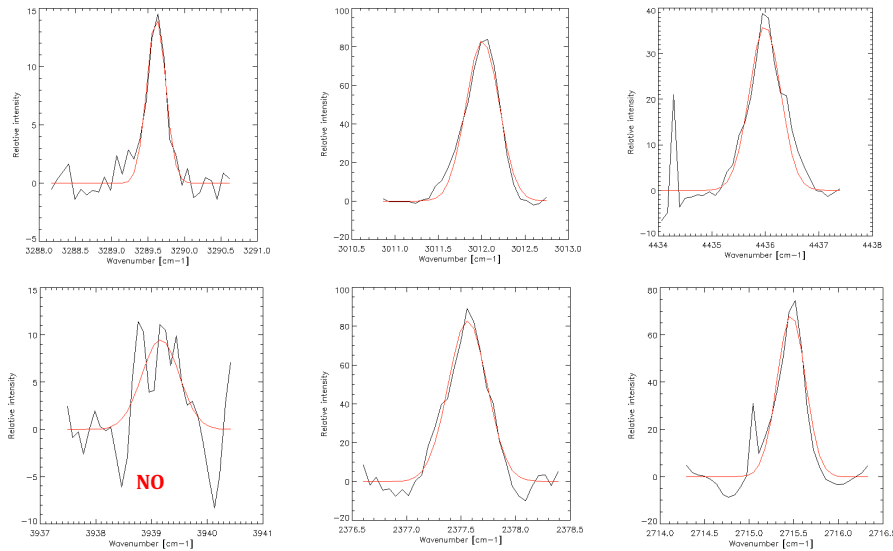


Figure 16 - Examples of solar lines from SO observations. Those marked with a 'NO' are discarded from retrieval.

3.2. Temperature dependency of wavenumber calibrations

The available observations have put in evidence that the instrumental temperature is subjected to significant variations. The dynamic ranges and absolute values of temperatures are generally different between SO and LNO configurations, as it appears at a first glimpse in Table 1. It has been observed that this temperature fluctuations are responsible for mechanical strain in the grating, which yields some displacement of the observed frequencies with respect to the performed calibration.

3.2.1. Temperature effects correction

The correction of these effects is performed using a mechanism analogous to that implemented in the first part of frequency calibration. The procedure, named *exotemp.pro*, uses all the observations available for a certain date (types M, C and F in Table 1, only D observations are excluded). For each individual spectrum in each file, the algorithm computes a first guess for frequencies vs. pixel number and order, based on the wavenumber calibration already performed for that date. Then, through the same correlation scheme (Eq. 3, 4) implemented in *exofreq.pro*, for each spectrum a displacement is computed with respect to the initial grid.

The results are retained only if:

- Solar lines above the defined threshold (see Section 3.1.1) in the spectrum are at least 2 and no more than 10. This condition is useful to exclude cases in which the number of lines does not suffice to perform a robust correlation, or makes the spectrum too rich of features, which can be too close one to each other.
- The displacement is lower than 10 pixels
- The correlation value for the single line (Eq. 4) exceeds 0.4
- The correlation value for the whole spectrum (Eq. 3) exceeds 0.1

As a last step, the procedure performs a polynomial fit between the displacements in pixels, Δp , and the temperature T (in °C) of the instrument. A second order polynomial is used, to be coherent with what is expected to be the effect of thermal stress:

$$\Delta p = Q_0 + Q_1T + Q_2T^2 \quad \text{Eq. 6}$$

3.2.2. Results

As already briefly mentioned in Section 2.2, for calibration purposes, the temperature is that registered by sensor 1 (under '/Housekeeping/SENSOR_1_TEMPERATURE_SO-LNO' field in the .h5 files), which has been observed to be more stable than that coming from the other sensors. To exemplify, Figure 17 shows an example of the temperatures available in a miniscan.

To cover the largest interval of temperatures and frequencies, a single fit has been performed, using all the files available and all the dates. Results for SO and LNO are reported in Figure 18. The coefficients of the polynomial relation in Eq. 6 are in Table 3. It is clear that the displacement with respect to the wavenumber calibration can reach values up to 8 pixels for SO (corresponding to $\sim 1 \text{ cm}^{-1}$ for the higher diffraction orders), and up to 5 pixels for LNO.

It has also to be stressed that, based on the fit residuals, this calibration guarantees that the possible residual error in the wavenumber calibration is limited to two pixels (maximum 0.23 cm^{-1} for the higher orders).

Since this procedure computes the perturbation on the current wavenumber to pixel solution, the *exotemp.pro* procedure is run in synergy with *exofreq.pro*, meaning that every time the tuning relation for a particular date (or set of dates) is modified, also the temperature correction parameterization expressed by Eq. 6 has to be adjusted.

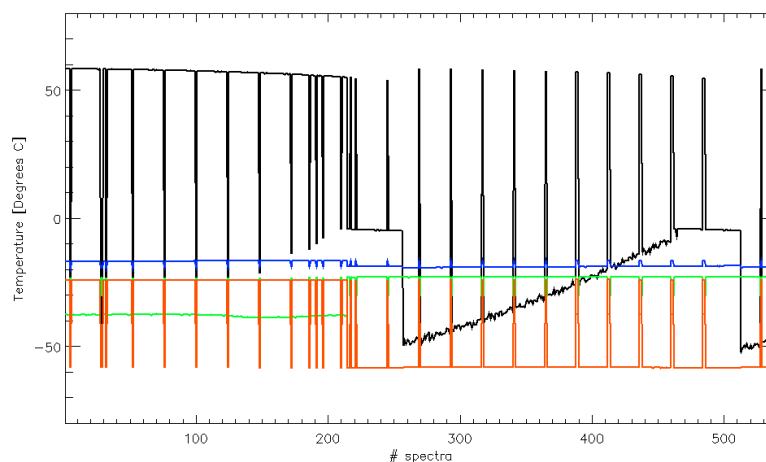


Figure 17 - Example of temperatures for the miniscan L13. Black plot: AOTF temperature; blue: Sensor 1; green: Sensor 2; red: Sensor 3. The Sensor 1 is the most stable.

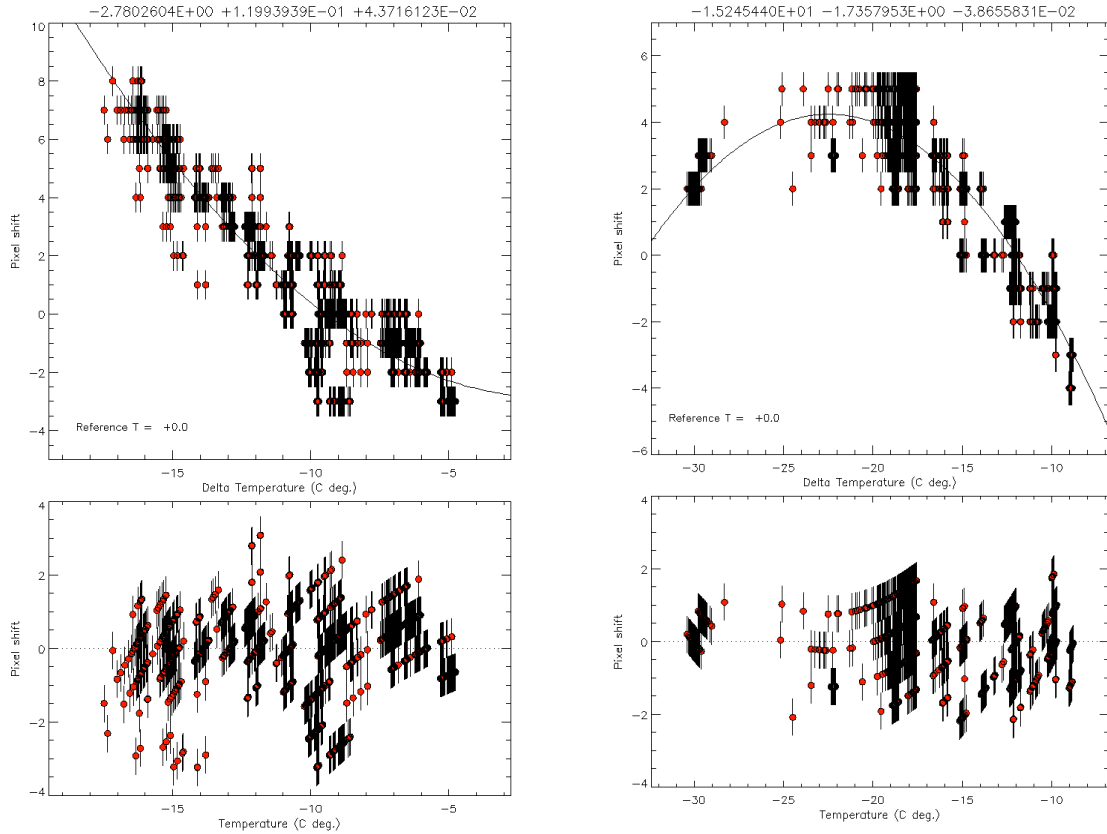


Figure 18 - Fits for the dependency of the frequency shift (in pixel, Y-axis) on the Sensor 1 temperature (Degrees C, X-axis). Each point corresponds to a single spectrum. SO is on the left, LNO on the right.

INSTRUMENT	DATE	Q_0	Q_1	Q_2
SO	All	-2.780260	$1.199394 \cdot 10^{-1}$	$4.371612 \cdot 10^{-2}$
LNO	All	-15.24544	$-1.735795 \cdot 10^{-4}$	$-3.865583 \cdot 10^{-2}$

Table 3 - Coefficients for the temperature dependency of wavenumber shift.

3.3. Wavenumber vs. AOTF frequency calibration and AOTF transfer function

The aim of this calibration procedure is to reckon the coefficients of the polynomial relation (see Eq. 2) between the AOTF input radio frequency and the central wavenumber of its bandpass. The algorithm has been implemented in the IDL routine *exoaotf.pro*.

3.3.1. Principles and implementation

Like for the grating equation, this calibration exploits the data from the miniscans, which span an AOTF frequency interval around 500 kHz. The basic idea is to track the depth of selected solar lines as AOTF frequency slightly varies. This will enable to describe both the shape of the AOTF transfer function as a function of wavenumber, and the AOTF frequency corresponding to the maximum sensitivity to the wavenumber at which solar line is located.

Like before, spectra are classified by order, using the same approach explained in Section 3.1.1. Since the AOTF calibration procedure is run after the frequency calibration, the spectral grid is calculated, for each order, using the coefficients F_0 , F_1 and F_2 already derived, and some a-priori (from previous calibrations) values for G_0 , G_1 and G_2 .

For each order, all the solar lines whose intensity is above a defined threshold are selected. Then, in order to perform homogeneous calculations independently of the order, the position of each selected solar line is described by wavenumber ν divided by order (denoted with ν').

Issues can arise in case there are two or more solar lines that fall within the same pixels, or too close one to each other. This occurrence has to be avoided especially when these solar lines fall in different diffraction orders, because in this case the line depth as a function of AOTF frequency will exhibit as many peaks as the number of superimposed solar lines of different orders.

To avoid this circumstance, the selected lines are sorted by ν' values, and those closer than the equivalent of 5 pixels are discarded.

The next step is, for each of the remaining $k = 1, \dots, N$ lines, to calculate the line depth as a function of the AOTF frequency A , with the double aim stated at the beginning of the Section. To do so, the algorithm extracts the 30 pixels around the center of the line, and uses the pixels free of any absorption line to compute the local continuum C_k around the k -th line, as a simple 3rd order polynomial. Then, the continuum is used to compute the integral $L_{d,k}(A)$ of line absorption, for each AOTF frequency A in the miniscan:

$$L_{d,k}(A) = \frac{1}{2\Delta\nu+1} \sum_{j=v_{0,k}-\Delta\nu}^{v_{0,k}+\Delta\nu} |C_k(j, A) - S(j, A)|, \quad k = 1, \dots, N \quad \text{Eq. 7}$$

where $\Delta\nu$ is the number of pixels around the line center used to compute the integral, and is one of the user-defined parameters of the procedure.

Each of the $L_{d,k}(A)$ functions is representative of the AOTF transfer function. By trials and errors, it has been found that the best way to represent the AOTF transfer function for NOMAD is the sum of a sinc-squared function, a gaussian, and a first order polynomial for the residual continuum. This model is much more simple than that adopted for the SOIR observations [4], that was based on the sum of 5 sinc-squared functions. Here the form of AOTF function model is as follows:

$$TF(\nu, \nu_0, I_0, w, I_G, \sigma_G, q, n) = F_{sinc} + F_{gauss} + F_{cntnm} \quad \text{Eq. 8}$$

$$\begin{cases} F_{sinc}(\nu, \nu_0, I_0, w) = I_0 w^2 \frac{\left[\sin \frac{\pi(\nu - \nu_0)}{w} \right]^2}{\pi^2 (\nu - \nu_0)^2} \\ F_{gauss}(\nu, \nu_0, I_G, \sigma_G) = I_G \exp \left[\frac{-(\nu - \nu_0)^2}{\sigma_G^2} \right] \\ F_{cntnm}(\nu, \nu_0, q, n) = q + n(\nu - \nu_0) \end{cases}$$

where:

- ν_0 is the center of the AOTF transfer function (in cm^{-1}). The first guess of this value is computed using the relation between ν_0 and A according to Eq. 2, using the prior coefficients;
- I_0 the sinc-squared amplitude;
- w the location of the first zero-crossing of the sinc-squared function; there is relation between w and the sinc-squared FWHM (which in this case is NOT straightforwardly the AOTF transfer function bandpass amplitude): $\text{FWHM} \approx 0.886 w$;
- I_G the gaussian amplitude;
- σ_G the gaussian standard deviation;
- q and n the offset parameters

In summary, the description of the AOTF transfer function is achieved, for each line, with a total of 7 parameters. The fit, performed through the *mpfitfun* IDL procedure, puts some constraints to retain or discard the result. The procedure retains only those lines for which:

- the fit converges (within 50 iterations)

- the error on ν_0 is lower than 5 cm^{-1}
- the value of ν_0 is within 20 cm^{-1} the first guess. This is useful both to avoid divergences, and to discard possible residual cases in which two lines of different diffraction orders fall within the same pixels. The 20 cm^{-1} threshold is chosen basing on the fact that the Free Spectral Range (FSR) of NOMAD is $\sim 22.5 \text{ cm}^{-1}$ (and is quantified by the F_0 coefficient previously derived).

3.3.2. Results: Wavenumber vs. AOTF frequency relation

The first goal of the procedure, namely the set of G_0 , G_1 and G_2 values of Eq. 2, are computed by polynomial fit of ν_0 vs. the corresponding AOTF frequency A at which the $L_{d,k}(A)$ function peaks. Figure 19 to Figure 24 show the results obtained using the miniscans available for single dates. Again, bottom panels report the residuals (in cm^{-1}) with respect to the best fit.

Figure 25 and Figure 26 illustrate the results obtained by gathering all the miniscans available for all the dates, and fitting results. The output coefficients, like for the tuning relation derived in Section 3.1, will be used as the standard to implement radiative transfer and retrievals over NOMAD data. All the sets of coefficients are reported in Table 4. The last two lines are dedicated to the results shown in Figure 25 and Figure 26.

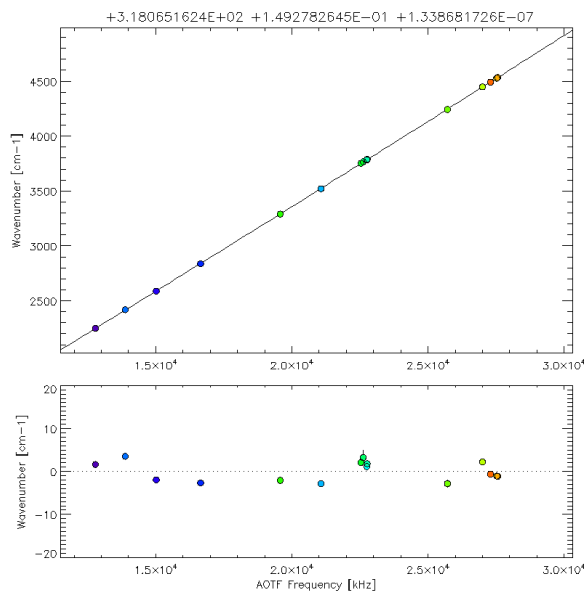


Figure 19 - Results for the SO miniscans of 22nd and 27th November 2016.

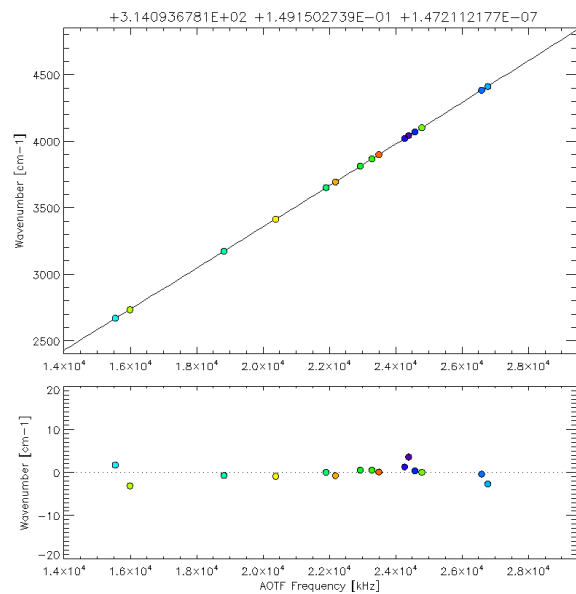


Figure 20 - Results for the SO miniscans of the 23rd November 2016.

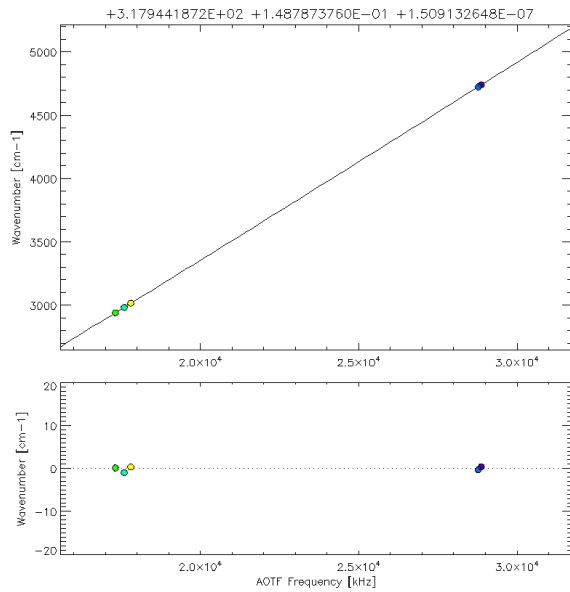


Figure 21 - Results for the SO miniscans of 25th November 2016.

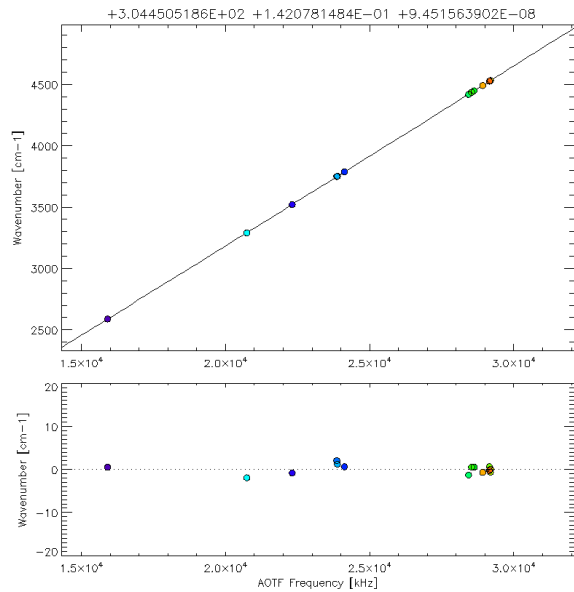


Figure 22 - Results for the LNO miniscans of the 22nd and 27th of November 2016

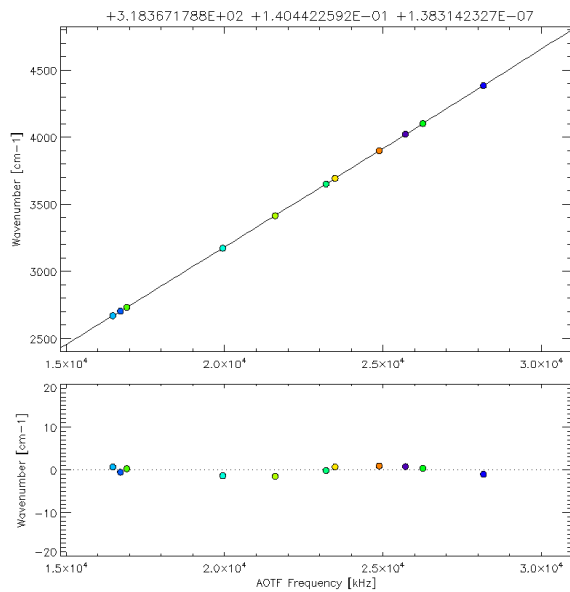


Figure 23 - Results for the LNO miniscans of the 23rd November 2016.

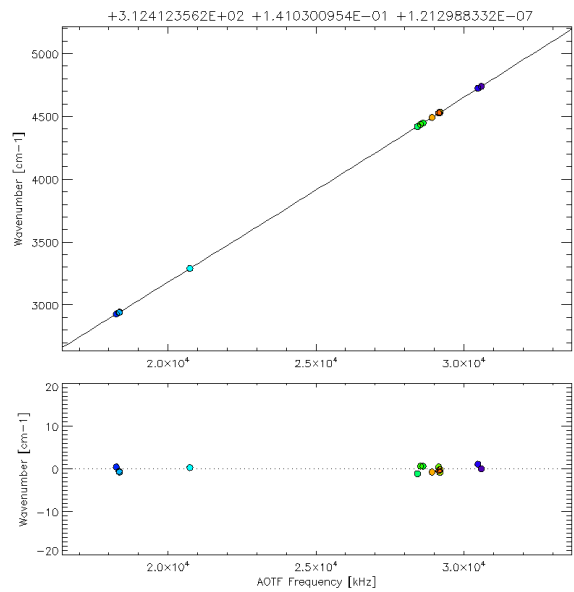


Figure 24 - Results for the LNO miniscans of the 25th and 27th November 2016.

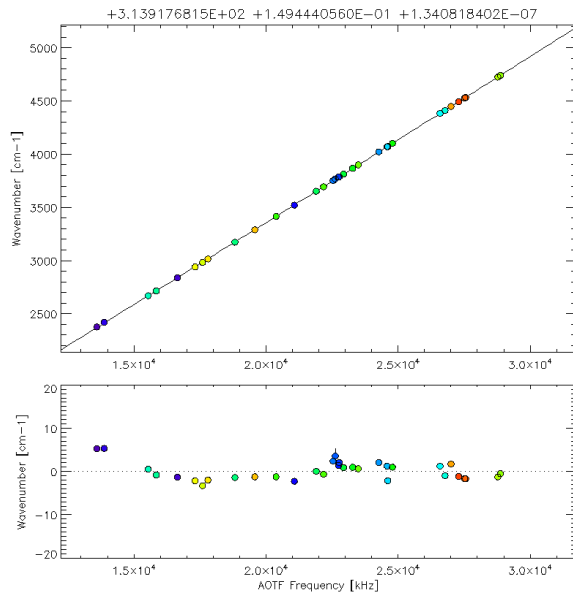


Figure 25 - Results for all the available SO miniscans in the four dates.

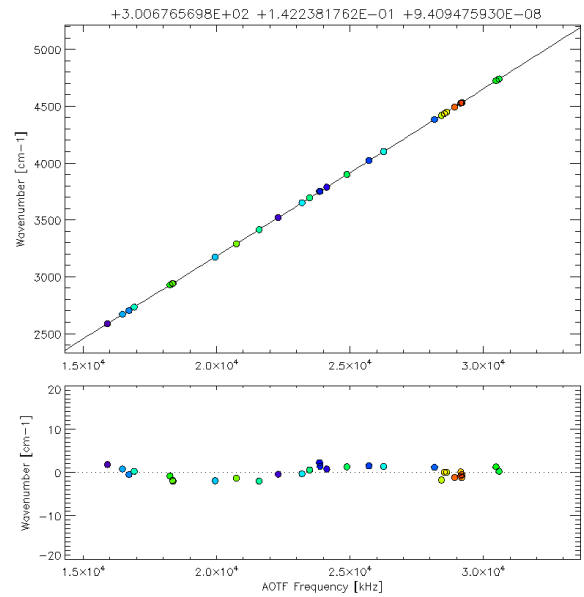


Figure 26 - Results for all the available LNO miniscans in the four dates.

INSTRUMENT	DATE	G_0	G_1	G_2
SO	22 nd -27 th Nov. 2016	318.06516	0.1492783	$1.338681 \cdot 10^{-7}$
SO	23 rd Nov. 2016	314.09368	0.1491503	$1.472112 \cdot 10^{-7}$
SO	25 th Nov. 2016	317.94418	0.1487874	$1.509133 \cdot 10^{-7}$
LNO	22 nd -27 th Nov. 2016	304.45052	0.1420781	$9.451564 \cdot 10^{-8}$
LNO	23 rd Nov. 2016	318.36718	0.1404423	$1.383142 \cdot 10^{-7}$
LNO	25 th -27 th Nov. 2016	312.41236	0.1410301	$1.212988 \cdot 10^{-7}$
SO	All	313.91768	0.1494441	$1.340818 \cdot 10^{-7}$
LNO	All	300.67657	0.1422382	$9.409476 \cdot 10^{-8}$

Table 4 - List of the wavenumber vs. AOTF frequency calibration coefficients obtained using miniscans of selected dates. The last two lines (bold) report the coefficients obtained using all the available miniscans.

3.3.3. Results - AOTF transfer function shape

Instead of deriving a variable AOTF transfer function shape (namely, describe the variability of this set of coefficients across all the orders), the procedure output consists of a single set of coefficients for all the miniscans (and the orders covered therein) in the selected dates. This is done taking all the lines for which the convergence conditions are satisfied, subtracting the continuum function derived from the fit, and re-centering all the $L_{d,k}(v)$ around zero, and computing their sum. The grand total of the single line transfer functions is then fitted again using the model described by the set of Eq. 8, with a-priori conditions $n=q=0$. This yields to a set of final parameters for the AOTF transfer function.

Results for the AOTF transfer function shape are illustrated in Figure 27 for SO (left) and LNO (right). These are obtained using all the miniscans of all the dates. The fitting parameters sets are provided in Table 5, where the three parameters correspond, respectively, to the position of the first zero-crossings of the sinc squared component of AOTF function (w), the width of the Gaussian component (σ_G), and the ratio between the Gaussian intensity and the sinc squared intensity (I_G/I_0).

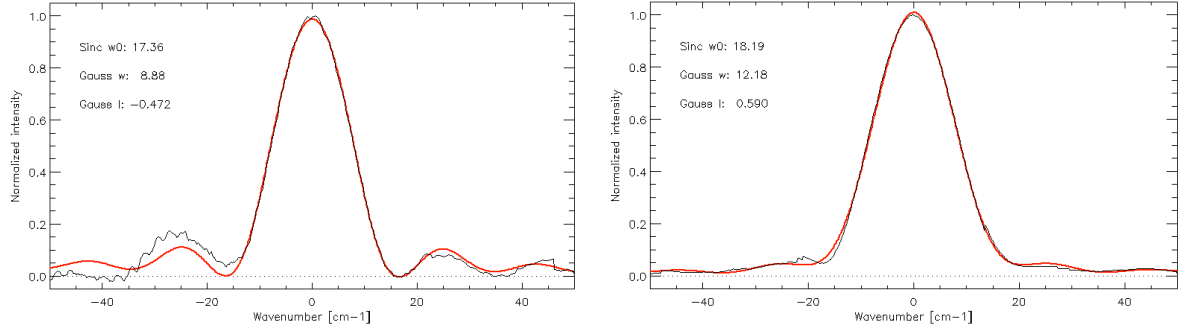


Figure 27 - Average AOTF transfer functions (black) derived from SO (left) and LNO (right) and corresponding fitted models (red).

INSTRUMENT	DATE	w	σ_G	I_G/I_0
SO	22 nd to 27 th Nov. 2016	17.358663	8.881119	-0.472221
LNO	22 nd to 27 th Nov. 2016	18.188122	12.181137	+0.589821

Table 5 - Retrieved coefficients for the shape of the AOTF transfer function.

Although the values of w cannot be directly related to the FWHM of the AOTF bandpass, it is clear that the two AOTFs have quite different properties, both in terms of width and shape of the transfer function. The negative value in the third coefficient for SO means that the best-fit Gaussian has a reversed shape with respect to the sinc squared, implying excess sidelobe contribution with respect to a regular sinc squared function.

4. Spectral continuum modeling

The spectra as observed by NOMAD in SO and LNO exhibit a continuum, whose shape is the result of the combined shape of the AOTF transfer function, and the grating efficiency due to blazing. The modeling of the spectral continuum is an essential part of the calibration process, especially in the interpretation of LNO nadir data, for which no reference measurements are possible, like in the case of SO occultations [1,4].

4.1. Blaze function

The blaze function is assumed to have a sinc-squared shape:

$$F_{blaze}(p, p_0, w_p) = w_p^2 \frac{\left[\frac{\sin(\pi(p-p_0)/w_p)}{w_p} \right]^2}{\pi^2(p-p_0)^2} \quad \text{Eq. 9}$$

where p is the pixel number (from 0 to 319), p_0 is the center of the function in pixel units, and w_p is the width of the blaze function. This last parameter is equal to the equivalent in pixels of the FSR, which is defined by F_0 , as already said. It has also been found that the central pixel of the blaze function, namely p_0 , slightly moves with the diffraction order m , according to the following equation:

$$p_0(m) = 160.25 + 0.23 \cdot m \quad \text{Eq. 10}$$

A contour plot of the blaze function as a function of diffraction orders is provided in Figure 28.

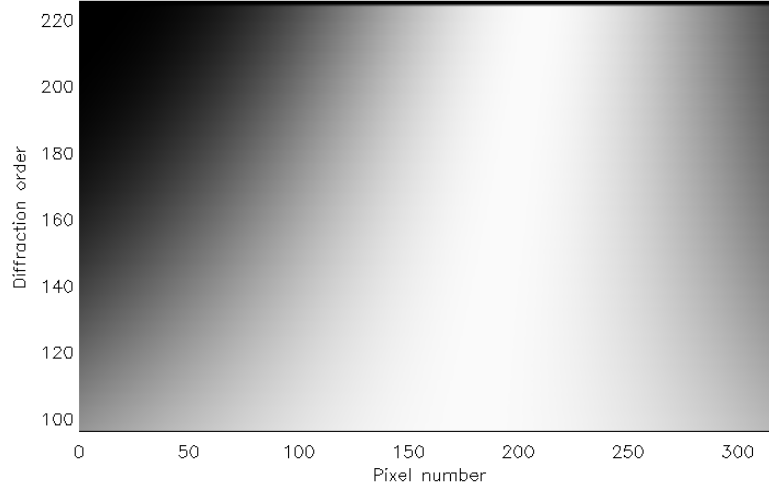


Figure 28 - Map of the relative intensity of the blaze function according to the order number and the pixel.

4.2. Structure of the spectral continuum

The model of the spectral continuum observed in NOMAD data has to take into account the flux coming from the “central” order (that in which AOTF function is centered) and the flux coming from a certain number of nearby orders, which can be as significant as 40% of the total signal. The contribution from each single order is equal to the product of the AOTF transfer function in that order by the blaze function of that order. Thus, the spectral continuum of a NOMAD spectrum acquired at an AOTF frequency A (the independent variable), whose corresponding wavenumber ν_0 is observed in the diffraction order m takes the subsequent form, here denoted with $PEC(A)$ (standing for Partial Elements Continuum, a function of the AOTF frequency):

$$PEC(A) = \sum_{j=m-\Delta m}^{m+\Delta m} PE(j) = \sum_{j=m-\Delta m}^{m+\Delta m} AOTF(A, \mathbf{v}_j) \cdot F_{blaze}(j, \mathbf{v}_j) \cdot gain(j) \quad Eq. 11$$

where $AOTF(A, \mathbf{v}_j)$ stands for the AOTF function at the AOTF frequency A , calculated on the spectral grid \mathbf{v}_j of the diffraction order j , $F_{blaze}(j, \mathbf{v}_j)$ is the blaze function of the diffraction order j , and $gain(j)$ is the spectral gain of the order j . However, if one considers a small amount Δm of orders around the central order m , the gain is not expected to dramatically vary, hence it can be put equal to 1 for every order, and the resulting normalized values of the $PEC(A)$ function will already represent the continuum of the NOMAD spectrum, normalized to the unity as well.

It has also been found that, despite the approach is that of retrieving a unique form for the AOTF transfer function, slight corrections are necessary for the SO to the width of the sinc squared component of that, w , with the order number m . The correction to the original w_0 value, reported in Table 5, takes the following form:

$$w(m) = w_0(1.23 - 5.5 \cdot 10^{-4} \cdot m) \quad Eq. 12$$

With this approach, it has been found that $\Delta m = 3$ is already adequate to represent the continuum of the NOMAD spectra of the datasets in Table 1. Sample comparisons between simulated continuum (through Eq. 11) and observed spectrum, at different AOTF frequencies, are provided in Figure 29 and Figure 30. The examples are taken from SO and LNO miniscans, to test the goodness of the model for different positions of the peak of the AOTF transfer function with respect to the blaze function of the central order.

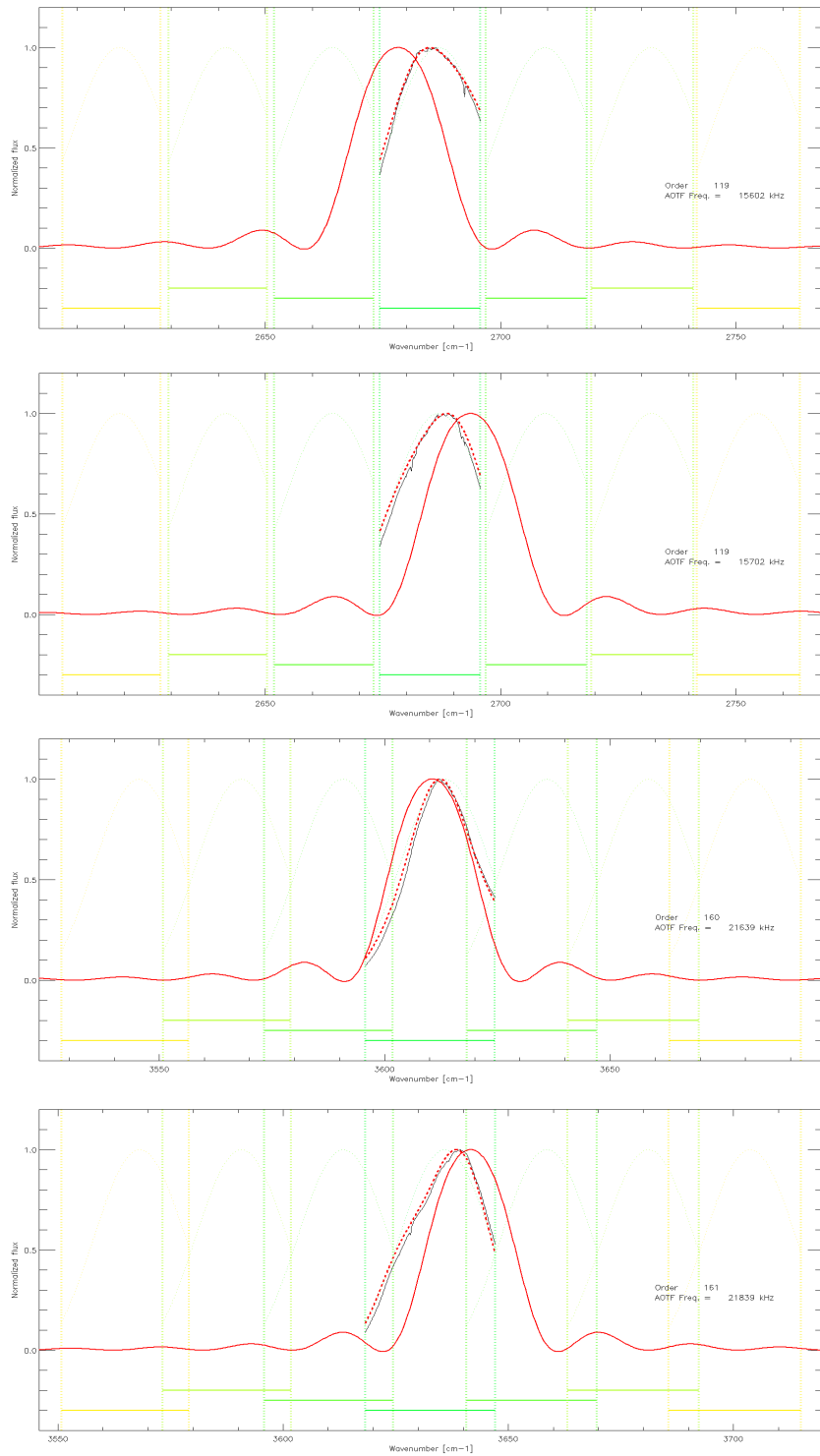


Figure 29 - Examples of simulated vs. observed continuum in NOMAD SO miniscan spectra (files #S15 and #S17, from the top). Red solid line: AOTF transfer function; Red dashed line: simulated continuum; Black line: observed NOMAD spectrum; Horizontal lines: central and nearby orders spectral intervals. Central order number and AOTF frequency at which the spectrum is acquired are also reported in each plot.

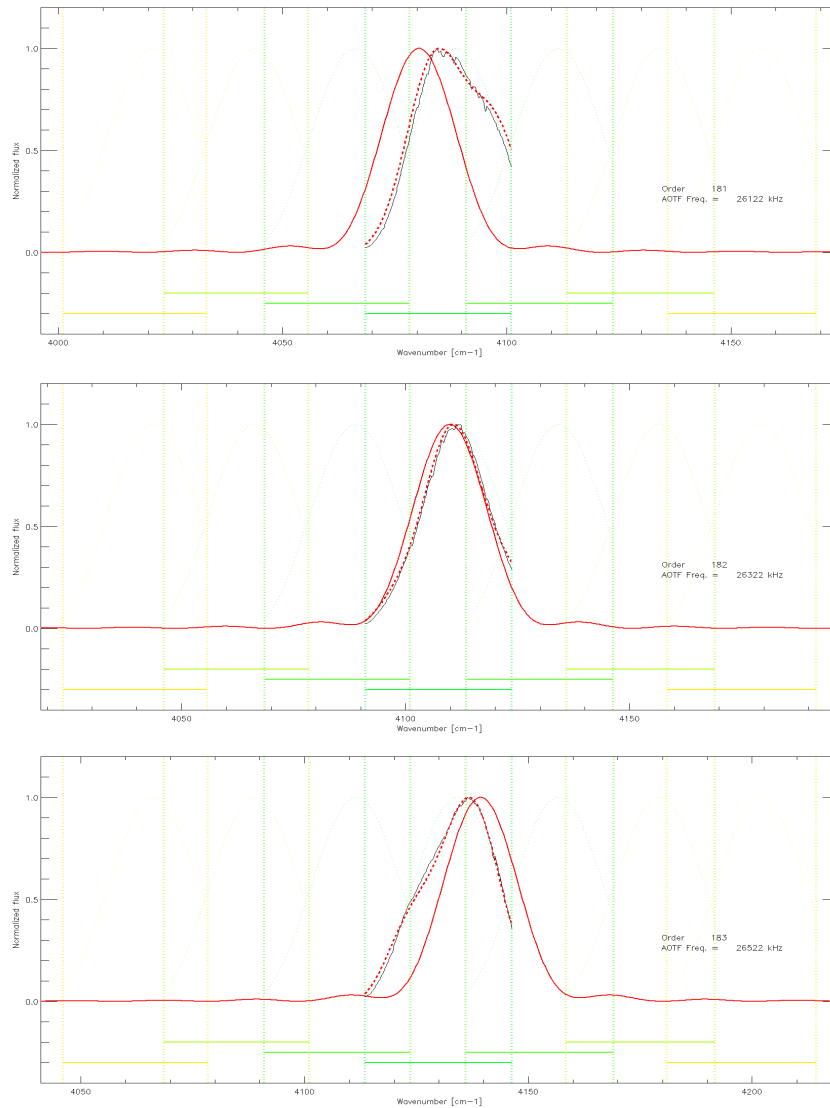


Figure 30 - As for figure 29, but for LNO miniscan data (file #L18).

The derivation of the continuum according to Eq. 11 is used also to quantify the amount of flux coming from the central and the nearby orders as the displacement between the peak of AOTF transfer function and the central pixel of the central order varies. A summary of this calculations is presented in Table 6 and Table 7 (for SO and LNO), in which it is shown that the contribution from nearby orders can reach 45% of the total flux for higher orders (this is also due to the significant overlap between the spectral intervals of nearby orders, increasing with order number).

The algorithm to compute the spectral continuum, whose core is Eq. 11, is implemented in the IDL function named *exocont.pro*, which takes in input the following parameters: the instrument (SO or LNO), the calibration coefficient defined so far (blaze function center included), the AOTF frequency, the temperature at which the spectrum is acquired, and the number of nearby orders to consider in the calculation of the continuum shape (Δm in Eq. 11).

ORDER	NEARBY ORDERS	AOTF CENTERED	AOTF FREQ. \pm 20 kHz	AOTF FREQ. \pm 50 kHz
100	Central	0.8340	0.7978	0.6264
	1 st nearby	0.1178	0.1500	0.3065
	2 nd nearby	0.0322	0.0357	0.0491
	3 rd nearby	0.0161	0.0165	0.0180
120	Central	0.7898	0.7545	0.5968
	1 st nearby	0.1602	0.1911	0.3339
	2 nd nearby	0.0352	0.0387	0.0502
	3 rd nearby	0.0148	0.0158	0.0192
140	Central	0.7366	0.7055	0.5700
	1 st nearby	0.2112	0.2379	0.3595
	2 nd nearby	0.0384	0.0414	0.0505
	3 rd nearby	0.0137	0.0152	0.0199
160	Central	0.6764	0.6542	0.5492
	1 st nearby	0.2680	0.2868	0.3810
	2 nd nearby	0.0421	0.0440	0.0496
	3 rd nearby	0.0135	0.0151	0.0202
180	Central	0.6137	0.6020	0.5328
	1 st nearby	0.3262	0.3367	0.4006
	2 nd nearby	0.0457	0.0459	0.0472
	3 rd nearby	0.0143	0.0154	0.0193
200	Central	0.5545	0.5505	0.5151
	1 st nearby	0.3796	0.3841	0.4214
	2 nd nearby	0.0499	0.0489	0.0453
	3 rd nearby	0.0160	0.0165	0.0182
220	Central	0.5051	0.5051	0.4966
	1 st nearby	0.4187	0.4221	0.4418
	2 nd nearby	0.0549	0.0527	0.0441
	3 rd nearby	0.0213	0.0201	0.0174

Table 6 - Summary of the contribution to the total observed flux from central and nearby orders according to the order (first column) and the displacement between the AOTF transfer function peak and the central pixel. Displacement is in AOTF frequency units (kHz). The table is for SO.

ORDER	NEARBY ORDERS	AOTF CENTERED	AOTF FREQ. \pm 20 kHz	AOTF FREQ. \pm 50 kHz
120	Central	0.8240	0.7886	0.6429
	1 st nearby	0.1564	0.1898	0.3299
	2 nd nearby	0.0140	0.0155	0.0199
	3 rd nearby	0.0056	0.0061	0.0073
140	Central	0.7680	0.7365	0.6126
	1 st nearby	0.2101	0.2402	0.3601
	2 nd nearby	0.0162	0.0171	0.0199
	3 rd nearby	0.0057	0.0062	0.0075
160	Central	0.7075	0.6847	0.5886
	1 st nearby	0.2681	0.2902	0.3843
	2 nd nearby	0.0184	0.0186	0.0196
	3 rd nearby	0.0061	0.0064	0.0075
180	Central	0.6467	0.6320	0.5642
	1 st nearby	0.3268	0.3417	0.4093
	2 nd nearby	0.0201	0.0196	0.0193
	3 rd nearby	0.0065	0.0066	0.0072
200	Central	0.5905	0.5818	0.5388

	1 st nearby	0.3811	0.3904	0.4342
	2 nd nearby	0.0214	0.0207	0.0200
	3 rd nearby	0.0070	0.0070	0.0070
220	Central	0.5461	0.5389	0.5142
	1 st nearby	0.4227	0.4298	0.4546
	2 nd nearby	0.0225	0.0225	0.0235
	3 rd nearby	0.0087	0.0088	0.0077

Table 7 - Same as table 6, but for LNO.

4.3. Synthetic spectra sample calculations

The calculation of the synthetic NOMAD radiances is entirely based on the calibration output coefficients and on the form of Eq. 11 for the continuum. Given m the central diffraction order (defined by the AOTF frequency A at which the spectrum is acquired), the spectrum is calculated in this way:

$$R(A, \mathbf{v}_m) = \sum_{j=m-\Delta m}^{m+\Delta m} PE(j) \cdot \tau(j, \mathbf{v}_j) = \sum_{j=m-\Delta m}^{m+\Delta m} AOTF(A, \mathbf{v}_j) \cdot F_{blaze}(j, \mathbf{v}_j) \cdot gain(j) \cdot \tau(j, \mathbf{v}_j) \quad Eq. 13$$

where the only new term with respect to Eq. 11 is the radiance spectrum of the observed system (atmosphere, atmosphere+surface, atmosphere+sun). In the subsequent examples, this term will be simply the solar reference spectrum, since we are dealing with calibration measurements. The radiance is computed by convolving the “infinite” resolution spectrum to the Instrumental Line Shape (ILS), whose FWHM is one of the output of the frequency calibration (see Section 3.1), which is different for SO and LNO. The FWHM of the ILS corresponds to a resolving power of ~ 19000 for SO and ~ 14000 for LNO, and is assumed to be a Gaussian profile (based on the investigations already done for SOIR).

In the following plots, a blend of simulated spectra vs. NOMAD observations is presented, together with the corresponding residuals and the solar spectrum for each of the nearby orders used. A value of $\Delta m=3$ is used.

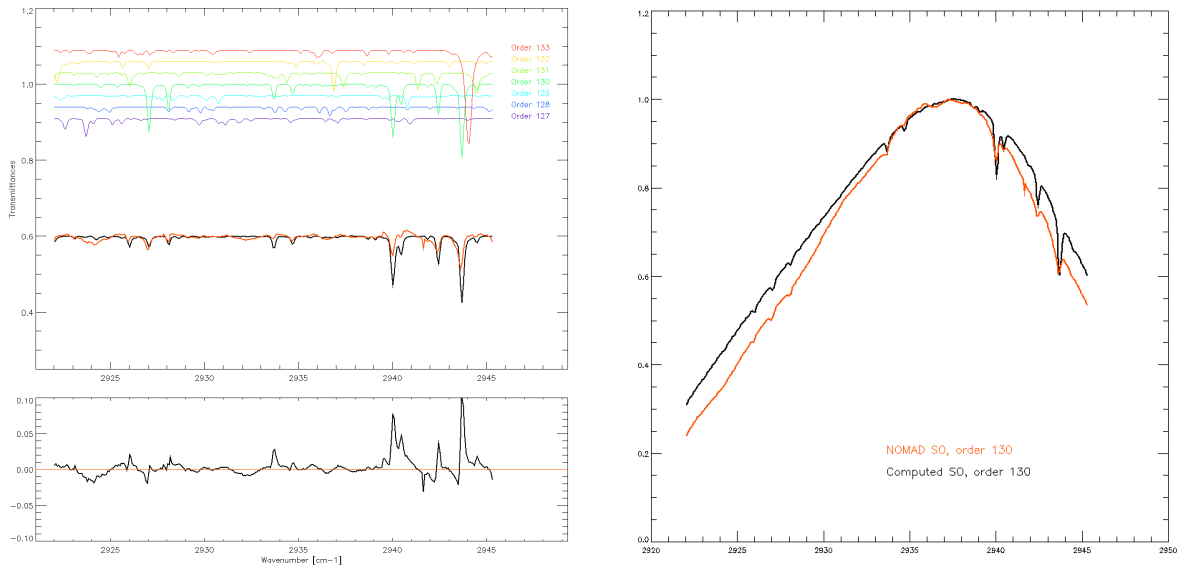


Figure 31 - Example of SO spectrum compared with the simulated one. Left panel: normalized observed spectrum (red) compared with the simulated (black), using Eq. 13, and summing up the contributions from single orders (top). Bottom panel: residuals in transmittance units. Right panel: comparison between the non-normalized spectra. The continuum

of the simulated spectrum (black) is computed via Eq. 11. Frequency solution is already corrected by the effect of temperature. The spectrum is one of the full scan #S5 in Table 1.

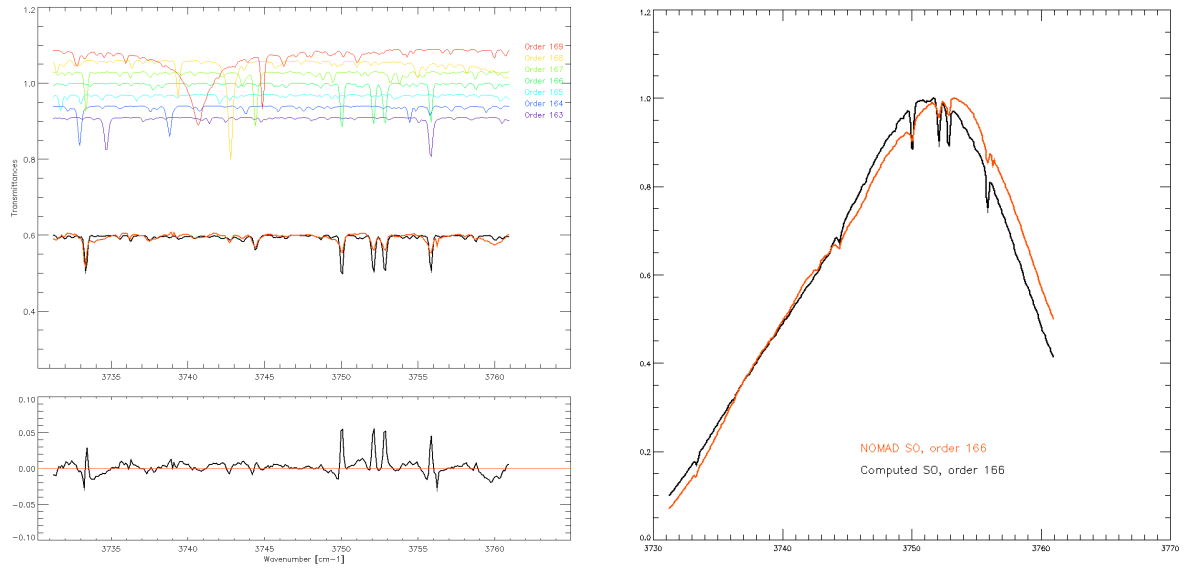


Figure 32 – As Figure 31, for another diffraction order of the same SO full scan (file #S5 in Table 1).

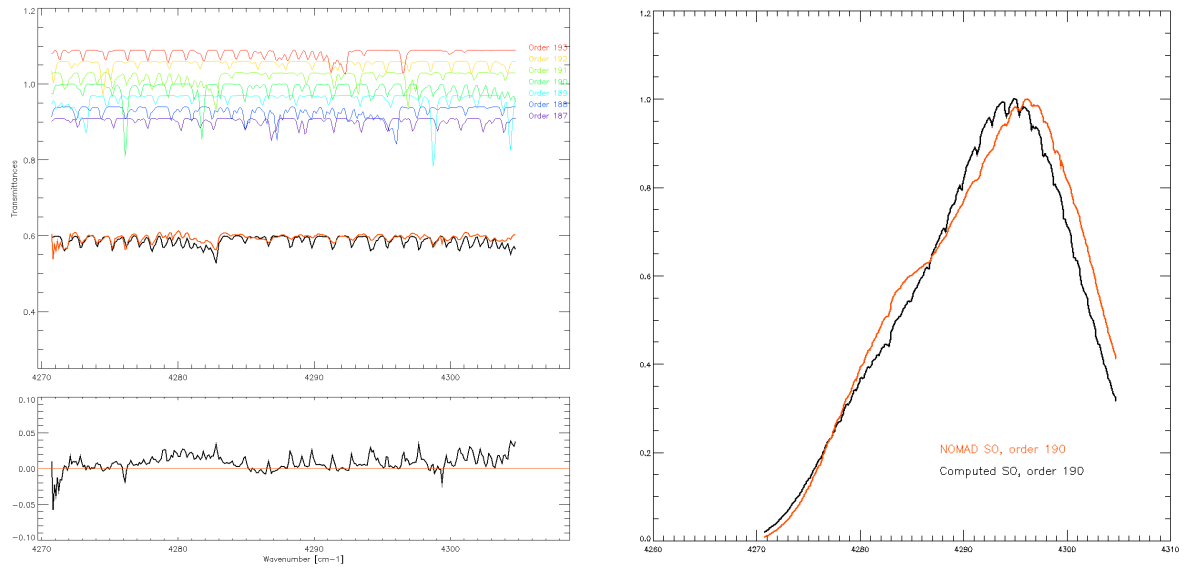


Figure 33 – As Figure 31, for another diffraction order of the same SO full scan (file #S5 in Table 1).

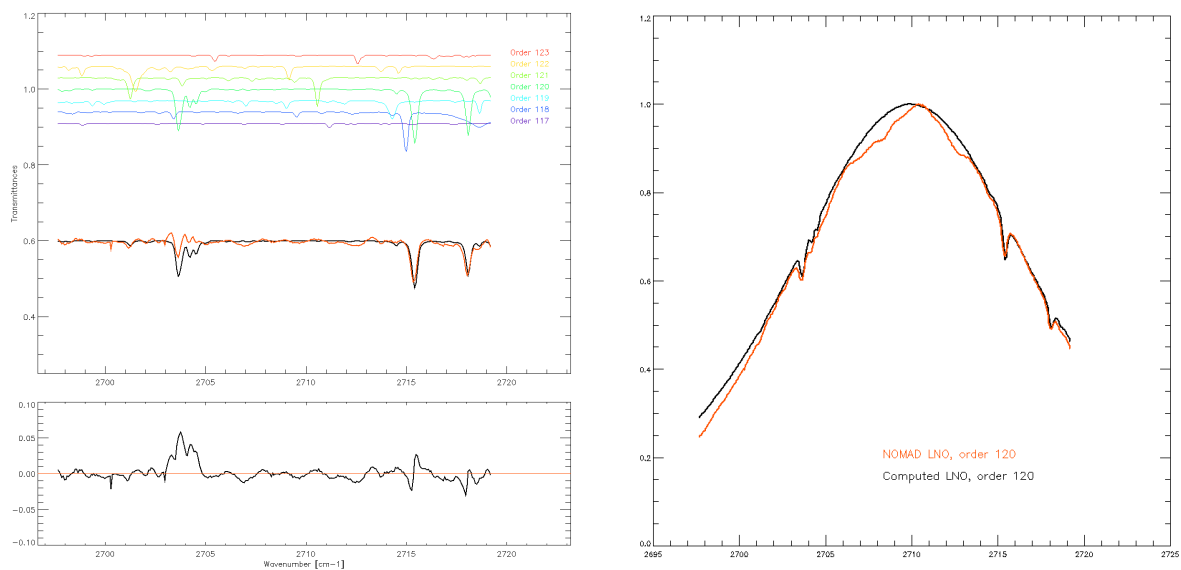


Figure 34 - As Figure 31, but for a spectrum acquired in LNO configuration. The spectrum is one of those acquired in the full scan #L6 (Table 1).

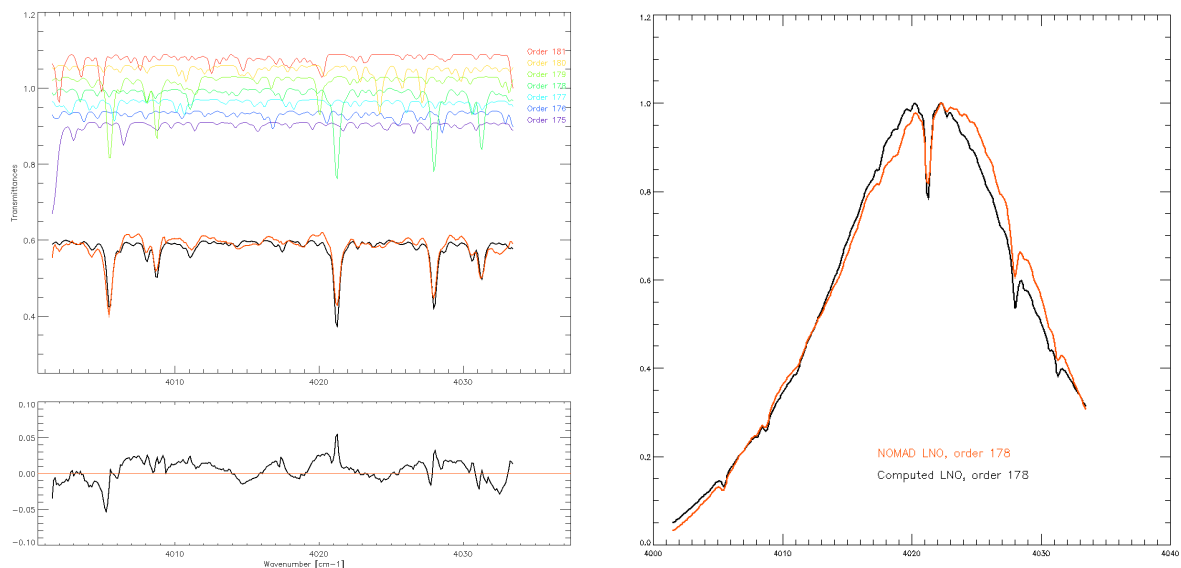


Figure 35 - As Figure 34, for another diffraction order of the same LNO full scan (file #L6 in Table 1).

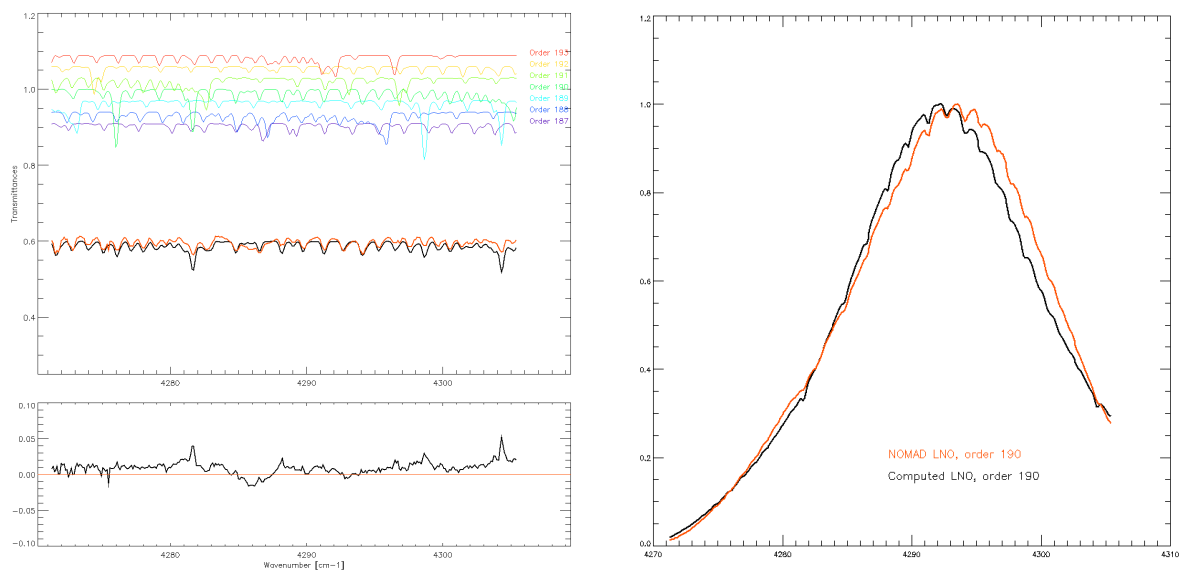


Figure 36 – As Figure 34, for another diffraction order of the same LNO full scan (file #L6 in Table 1).

The spectra shown here in Figure 31 to Figure 36 put in evidence that:

- In LNO data, a Gaussian line profile does not generate any significant bias in the residuals.
- The temperature correction proves to be adequate at a level of precision of ± 2 pixels, as already evidenced in the analysis in Section 3.2.
- SO spectra exhibit a clear variation of sharpness in the spectral features, which dramatically decreases along the wavenumbers covered by the single order, with respect to simulated spectra (see e.g. Figure 33). This effect is common to all the diffraction orders.

5. Conclusions and future work

This report has described all the calibration procedures on the NOMAD instrument performed. Both the grating and AOTF quantitative properties have been characterized. The overall sets of coefficients derived for SO and LNO are reported in Appendix A.

Future work will focus on the following topics and issues:

- Further validation of the Gaussian line profile;
- Radiative transfer exercises and retrievals on NOMAD LNO day nadir (D) data;
- Efforts to model the spectral quality degradation in SO observations;
- Periodic verification of the calibration parameters retrieved so far as new calibration miniscan (M) observations come.
- Individuation of the optimal AOTF frequencies to maximize the SNR in wavenumbers of interest for the retrieval of specific gases and organics.

Appendix B reports the table of the “optimal” AOTF frequencies per diffraction order: based on the calibration performed so far, the table contains those AOTF frequencies which yield an AOTF transfer function co-centered with the blaze function. For comparison, the current AOTF full scan frequencies are reported. In case of SO, they can be quite different (~ 30 kHz forward) and need to be adjusted (see e.g the example in the Figure in Appendix B for SO).

References

- [1] Vandaele, A. C. et al., "Improved calibration of SOIR/Venus Express spectra", Optics Express, vol. 21 (18), 21148 - 21161, 2013, [doi:10.1364/OE.21.021148](https://doi.org/10.1364/OE.21.021148)
- [2] Nevejans, D. et al., "Compact high-resolution space-borne echelle grating spectrometer with AOTF based on order sorting for the infrared domain from 2.2 to 4.3 μm ", Applied Optics, vol. 45 (21), 5191 - 5206, 2006, [doi: 10.1364/AO.45.005191](https://doi.org/10.1364/AO.45.005191)
- [3] Neefs, E. et al., "NOMAD spectrometer on the ExoMars trace gas orbiter mission: part 1—design, manufacturing and testing of the infrared channels", Applied Optics, vol. 54 (28), 8494 - 8520, 2015, [doi: 10.1364/AO.54.008494](https://doi.org/10.1364/AO.54.008494)
- [4] Mahieux, A. et al., "In-flight performance and calibration of SPICAV SOIR onboard Venus Express", Applied Optics, vol. 47 (13), 2252 - 2265, 2008, [doi: 10.1364/AO.47.002252](https://doi.org/10.1364/AO.47.002252)

Appendix A – Calibration coefficients

Calibration relations:

The relations for calibration are Eqs. 1, 2, 6 and 8. Summary of the coefficients for SO and LNO:

SO	Frequency (F_0, F_1, F_2)	22.473422	$5.559526 \cdot 10^{-4}$	$1.751279 \cdot 10^{-8}$
	AOTF - Freq. (G_0, G_1, G_2)	313.91768	0.1494441	$1.340818 \cdot 10^{-7}$
	AOTF transfer ($w, \sigma_G, I_G / I_0$)	17.358663	8.881119	-0.472221
	Temperature (Q_0, Q_1, Q_2)	-2.780260	$1.199394 \cdot 10^{-1}$	$4.371612 \cdot 10^{-2}$
LNO	Frequency (F_0, F_1, F_2)	22.478113	$5.508335 \cdot 10^{-4}$	$3.774791 \cdot 10^{-8}$
	AOTF - Freq. (G_0, G_1, G_2)	300.67657	0.1422382	$9.409476 \cdot 10^{-8}$
	AOTF transfer ($w, \sigma_G, I_G / I_0$)	18.188122	12.181137	+0.589821
	Temperature (Q_0, Q_1, Q_2)	-15.24544	$-1.735795 \cdot 10^0$	$-3.865583 \cdot 10^{-2}$

Appendix B – AOTF optimal frequencies table

Order number	SO AOTF Freq. (kHz)		LNO AOTF Freq. (kHz)	
	This work	Current	This work	Current
96	12265	12316		
97	12413	12463		
98	12561	12610		
99	12709	12757		
100	12857	12905		
101	13004	13052		
102	13152	13199		
103	13300	13346		
104	13447	13493		
105	13595	13640		
106	13742	13787		
107	13890	13934		
108	14038	14081	14886	14878
109	14185	14228	15042	15034
110	14332	14375	15197	15190
111	14479	14521	15353	15346
112	14627	14668	15509	15502

113	14774	14815	15664	15658
114	14921	14962	15820	15814
115	15069	15109	15975	15970
116	15216	15255	16131	16126
117	15363	15402	16287	16281
118	15510	15549	16442	16437
119	15657	15695	16598	16593
120	15804	15842	16753	16749
121	15951	15988	16909	16904
122	16098	16135	17064	17060
123	16245	16281	17219	17215
124	16392	16428	17375	17371
125	16539	16574	17530	17527
126	16686	16721	17685	17682
127	16832	16867	17841	17837
128	16979	17014	17996	17993
129	17126	17160	18151	18148
130	17273	17306	18306	18304
131	17419	17453	18461	18459
132	17566	17599	18616	18614
133	17712	17745	18771	18769
134	17859	17892	18927	18924
135	18005	18038	19082	19080
136	18152	18184	19236	19235
137	18298	18330	19391	19390
138	18445	18476	19547	19545
139	18591	18622	19701	19700
140	18737	18768	19856	19855
141	18883	18914	20011	20010
142	19030	19060	20166	20165
143	19176	19206	20321	20319
144	19322	19352	20475	20474
145	19468	19498	20630	20629
146	19614	19644	20784	20784
147	19761	19790	20940	20938
148	19907	19936	21094	21093
149	20052	20082	21249	21248
150	20198	20228	21403	21402
151	20344	20373	21557	21557
152	20490	20519	21712	21711
153	20636	20665	21867	21866
154	20782	20810	22021	22020
155	20927	20956	22175	22174
156	21074	21102	22330	22329
157	21219	21247	22484	22483
158	21365	21393	22639	22637
159	21510	21539	22793	22792
160	21656	21684	22948	22946
161	21802	21830	23102	23100
162	21947	21975	23256	23254
163	22093	22121	23410	23408
164	22238	22266	23564	23562
165	22384	22411	23719	23716
166	22529	22557	23873	23870
167	22674	22702	24026	24024
168	22820	22847	24180	24178
169	22965	22993	24335	24332

170	23110	23138	24489	24486
171	23255	23283	24643	24640
172	23401	23428	24796	24793
173	23546	23574	24951	24947
174	23691	23719	25105	25101
175	23836	23864	25258	25254
176	23981	24009	25412	25408
177	24126	24154	25566	25562
178	24271	24299	25720	25715
179	24416	24444	25873	25869
180	24561	24589	26027	26022
181	24706	24734	26181	26175
182	24851	24879	26335	26329
183	24996	25024	26488	26482
184	25140	25169	26642	26635
185	25285	25314	26795	26789
186	25430	25459	26949	26942
187	25575	25603	27103	27095
188	25719	25748	27256	27248
189	25864	25893	27409	27401
190	26008	26038	27562	27555
191	26153	26182	27716	27708
192	26297	26327	27870	27861
193	26442	26472	28023	28014
194	26586	26616	28176	28166
195	26731	26761	28330	28319
196	26875	26906	28483	28472
197	27019	27050	28636	28625
198	27163	27195	28789	28778
199	27308	27339	28943	28931
200	27452	27484	29096	29083
201	27596	27628	29249	29236
202	27740	27772	29402	29389
203	27884	27917	29554	29541
204	28029	28061	29708	29694
205	28173	28205	29861	29846
206	28317	28350	30014	29999
207	28461	28494	30167	30151
208	28605	28638	30320	30304
209	28749	28782	30473	30456
210	28893	28927	30625	30608
211	29036	29071	30778	30761
212	29181	29215	30932	30913
213	29324	29359	31084	31065
214	29468	29503	31237	31217
215	29611	29647	31389	31369
216	29755	29791	31542	31521
217	29899	29935	31695	31674
218	30043	30079	31848	31826
219	30186	30223	32000	31978
220	30329	30367	32152	32130
221	30474	30511		
222	30617	30655		
223	30760	30799		
224	30903	30943		
225	31047	31086		

